Title
Summertime tropospheric observations related to N_xO_y distributions and partitioning over Alaska: Arctic Boundary Layer Expedition 3A

Journal
Journal of Geophysical Research, 97(D15)

ISSN
0148-0227

Authors
Sandholm, ST
Bradshaw, JD
Chen, G
et al.

Publication Date
1992-10-30

DOI
10.1029/92jd01491

JOURNAL OF GEOPHYSICAL RESEARCH, VOL. 97, NO. D15, PAGES 16,481–16,509, OCTOBER 30, 1992

Summertime Tropospheric Observations Related to N_xO_y Distributions and Partitioning Over Alaska: Arctic Boundary Layer Expedition 3A

S. T. SANDHOLM,[1] J. D. BRADSHAW,[1] G. CHEN,[1] H. B. SINGH,[2] R. W. TALBOT,[3,4] G. L. GREGORY,[3] D. R. BLAKE,[5] G. W. SACHSE,[5] E. V. BROWELL,[3] J. D. W. BARRICK,[3] M. A. SHIPHAM,[3] A. S. BACHMEIER,[6] AND D. OWEN[7]

Measurements of the reactive odd nitrogen compounds NO, NO_2, peroxyacetyl nitrate (PAN), and NO_y are presented for the summertime middle/lower troposphere (6.1–0.15 km) over northern high latitudes. In addition, the chemical signatures revealed from concurrent measurements of O_3, CO, C_2H_2, C_2H_6, C_3H_8, C_2Cl_4, and H_2O are used to further characterize factors affecting the budget and distribution of N_xO_y in the Arctic and sub-Arctic tropospheric air masses sampled over Alaska during the NASA Arctic Boundary Layer Expedition (ABLE 3A) field campaign. Many of the compounds listed above exhibited a general trend of median mixing ratios increasing in proportion with altitude within the lower 6-km column. However, median mixing ratios of NO and NO_x (NO + NO_2) were nearly independent of altitude, having values of about 8.5 and 25 pptv, respectively. Median mixing ratios of NO_y varied from about 350 pptv within the lowest altitudes to about 600 pptv within the highest altitudes sampled. PAN constituted the largest fraction of NO_y (~50%) at the highest altitudes. In addition, PAN mixing ratios accounted for all of the approximate 60 pptv/km altitudinal dependency in NO_y. The analyses presented implicate biomass burning in Siberia as the probable source of about one-third of the NO_y abundance within the middle/lower troposphere over Alaska. These analyses also implicate the downward transport of air from altitudes in the vicinity of the tropopause as a major contributor to the abundance of NO_y (~30–50%) within the lower 6-km column over Alaska. However, the exact origin of this high-altitude NO_y remains uncertain. The impact of lower latitude industrial/urban pollution also remains largely uncertain, although various chemical signatures imply inputs from these regions would have been relatively well aged (15–30 days).

1. INTRODUCTION

During the summertime, Alaska is situated between the Arctic and polar jets, resulting in air mass compositions affected by the mixing of cold Arctic air with warmer North Pacific maritime air. Consequently, Alaska constantly receives air masses having 2–5 day transits from areas that are relatively free of major anthropogenic pollution sources. This suggests that the Alaska troposphere should be relatively free of short-lived compounds (e.g., NO, NO_2, C_3H_6) originating from anthropogenic sources [e.g., *Miller*, 1981; *Patterson and Husar*, 1981; *Shaw*, 1981, 1988; *Carlson*, 1981; *Rahn*, 1981; *Raatz et al.*, 1985]. However, longer-lived compounds that typically have a free tropospheric lifetime of weeks to months (e.g., O_3, CO, CFCs, C_2H_2, C_2Cl_4) can be transported to Alaska from anthropogenic source regions located thousands of kilometers away. Transport times ranging from 1 to 3 weeks can spread such source influences from mesoscale to Arctic-scale dimensions [e.g., *Shaw*, 1981; *Patterson and Husar*, 1981].

The chemical composition of Alaska's troposphere can also be significantly influenced by naturally occurring sources of trace gases. Stratosphere-troposphere exchange can occur through several mechanisms, such as tropopause folding associated with jet streaks and the Polar and the Arctic jet streams, large-scale subsidence, and the development of cut-off lows. All of these mechanisms can provide inputs of O_3 and other trace gases to the middle troposphere. The peak activity in such processes begins in early spring and extends into summer [e.g., *Danielson*, 1968; *Raatz et al.*, 1985; *Shapiro et al.*, 1987; *Reiter*, 1975; *Vaughn and Price*, 1989; *Ebel et al.*, 1991]. Biomass burning in sub-Arctic regions releases a variety of trace gases to the atmosphere. Most of the area burned in these regions is the result of naturally occurring fires, which can be promoted during later phases of ecosystem succession [*Van Wagner*, 1988; *Chapin and Shaver*, 1985; *Stocks*, 1991]. This natural source of trace gases may significantly influence the chemical characteristics of the Alaskan summer troposphere. Intermixing these near and distance sources can result in a complex matrix representing both natural and anthropogenic influences on the troposphere over Arctic and sub-Arctic Alaska. The distribution and abundance of "reactive" odd nitrogen compounds (N_xO_y) originating from these sources can significantly influence tropospheric photochemistry in these environments.

The N_xO_y family of reactive odd nitrogen compounds contains both highly reactive compounds (e.g., NO, NO_2, and NO_3), reservoir compounds (e.g., peroxyacetyl nitrate (PAN), HO_2NO_2, and N_2O_5), and compounds that act as virtual sinks (e.g., HNO_3 and particulate-nitrate (p-NO_3^-)). In remote regions free from significant direct sources, tropospheric NO and NO_2 concentrations are often small (mixing ratios <25 pptv) [e.g., *McFarland et al.*, 1979;

[1]School of Earth and Atmospheric Sciences, Georgia Institute of Technology, Atlanta.
[2]NASA Ames Research Center, Moffett Field, California.
[3]NASA Langley Research Center, Hampton, Virginia.
[4]Now at Institute for the Study of Earth, Oceans, and Space, University of New Hampshire, Durham.
[5]Department of Chemistry, University of California at Irvine.
[6]Planning Research Corporation, Hampton, Virginia.
[7]S. T. Systems Corporation, Hampton, Virginia.

Paper number 92JD01491.
0148-0227/92/92JD-01491$05.00

Ridley et al., 1989; *Carroll et al.*, 1990]. Even at these small abundances, NO_x ($NO + NO_2$) is believed to be the most reactive component of the N_xO_y family. NO_x therefore plays a pivotal role in odd oxygen and odd nitrogen related photochemistry [e.g., *Levy*, 1972; *Logan*, 1985; *Lin et al.*, 1988]. Numerous researchers have described a significant portion of the nonurban troposphere as being NO_x limited in terms of the photochemical production of tropospheric oxidants. Specifically, increases in the tropospheric concentration of NO_x, above those concentrations that would naturally occur, will result in an anthropogenically derived increase in the abundance of tropospheric O_3 through the photochemical cycling of NO and peroxy radicals [e.g., *Logan*, 1985; *Liu et al.*, 1987].

The potential anthropogenic sources of N_xO_y compounds affecting the regions studied include regional-scale transport from Alaska's population centers, high-altitude aircraft, and long-range transport from industrial/urban centers in Europe, Asia, the North Pacific rim, and North America. Significant uncertainty can be associated with the determination of the role of long-rang transport of N_xO_y compounds from these mid-latitude continental source regions. For example, under summertime photochemical conditions, the rapid oxidation (on the order of hours) of NO_x to form HNO_3 may represent a significant loss pathway for tropospheric N_xO_y via wet and dry removal of HNO_3. Loss of HNO_3 in this manner could limit the long-range transport of N_xO_y compounds [e.g., *Logan et al.*, 1981; *Logan*, 1983]. In a companion paper, *Wofsy et al.* [this issue] propose that this type of mechanism may have reduced the impact of mid-latitude industrial/urban sources on the summertime N_xO_y budget in the middle/lower troposphere over several high-latitude regions.

PAN and other alkyl nitrates have been suggested as longer-lived reservoirs of N_xO_y compounds that may survive long-range transport to remote regions [e.g., *Crutzen*, 1979; *Singh and Hanst*, 1981; *Singh and Salas*, 1983; *Singh*, 1987; *Atlas*, 1988; *Douglass et al.*, 1989; *Madronich and Calvert*, 1990]. Indeed, a substantial burden of both PAN and NO_y was measured over most of the high-latitude regions studied in the Arctic Boundary Layer Expedition (ABLE 3) program (where NO_y represents the N_xO_y compounds measured using an Au catalytic convertor). It has been suggested that a large fraction of the measured high-latitude midtropospheric burden of these compounds may have been due to anthropogenic inputs [*Jacob et al.*, this issue; *Singh et al.*, this issue (*b*)]. Even so, PAN produced in regions of localized mid-latitude anthropogenic pollution may have limited ability to survive long-range transport during the warmer summer months due to its thermal instability. In addition, continuous input of precursor compounds may be necessary for the buildup and maintenance of large NO_y abundances during long-range transport [cf. *Atherton and Penner*, 1990; *Madronich and Calvert*, 1990]. A priori evaluation of the scope of anthropogenic influence on the Alaskan Arctic and sub-Arctic regions can not be reliably predicted based upon present knowledge, and considering the variety of naturally occurring N_xO_y sources affecting these regions.

NASA's ABLE 3A, conducted in July–August of 1988, had as its primary goal the comprehensive characterization of trace gas distributions and their sources/sinks in the summertime troposphere over the Arctic and sub-Arctic regions of North America [*Harriss et al.*, this issue (*a*)]. We present in this paper an examination of the factors affecting the N_xO_y distributions and partitioning of NO, NO_2, PAN, HNO_3, and NO_y measured in the Alaskan Arctic and sub-Arctic troposphere from 0.15 to 6.1 km during the ABLE 3A field program. Segregation of this data set into air mass types and origins was based on the meteorological synopses and air mass trajectory analyses of *Shipham et al.* [this issue] and the ABLE 3A data archive. In addition, the O_3 and aerosol and vertical structure information, provided by a lidar remote sensing instrument, aided identification of atmospheric pollution layers, mixed layer height, cloud cover, and regions of stratospheric/tropospheric exchange. Temporally coincident measurements of O_3, CO, C_2H_2, C_2H_6, C_3H_8, and C_2Cl_4 (as well as dew point, temperature, altitude, etc.) are also presented to further characterize the chemical structure of the various air masses sampled, and to obtain a greater understanding of potential sources affecting these regions. The entire ABLE 3A data set is available from NASA Global Tropospheric Experiment Program Office (Langley Research Center, Hampton, VA 23665).

2. Measurement Techniques

Detailed descriptions of the chemiluminescence O_3 system [*Gregory et al.*, this issue], the tunable diode laser absorption CO and CH_4 system [*Harriss et al.*, this issue (*b*)], the nonmethane hydrocarbon (NMHC) grab sample/analysis system [*Blake et al.*, this issue], the cryo-trap/GC-ECD PAN system [*Singh et al.*, this issue (*a*)], and the mist chamber-IC HNO_3 system [*Talbot et al.*, this issue], have been described elsewhere. NO, NO_2, and NO_y were measured simultaneously using the two-photon/laser-induced fluorescence technique (TP/LIF). Only the salient features of this latter technique are discussed in this section, as the technique has been previously described [*Bradshaw et al.*, 1985; *Sandholm et al.*, 1990].

The 226-nm and 1.1-μ laser beams that were used in the two-photon fluorescence excitation process were passed through three separate ambient sampling cells. One cell was designated for detecting ambient NO. A second cell was designated for detecting NO produced from the photolytic conversion of ambient NO_2. The third cell was designated for detecting NO produced from a gold catalytic conversion of ambient NO_y. Each of the three cells was equipped with its own fluorescence detection and gated photon counting systems. Simultaneous measurement capabilities using TP/LIF for NO and NO_2 have been previously described [*Sandholm et al.*, 1990]. Both the NO and NO_2 measurement systems have undergone critical intercomparison during the NASA/GTE Chemical Instrumentation Test and Evaluation Program I and II [*Hoell et al.*, 1984, 1987; *Gregory et al.*, 1990*a*, *b*].

The NO_2 photolytic convertor system uses a XeF excimer laser capable of producing high conversion efficiencies (typically 50–65%), with short total sample residence times (<2 s). The sample residence time through the NO portion of the system was always less than 1 s. These residence times were short enough to minimize potential artifacts associated with the back titration of either ambient NO or photolytically produced NO via reaction with ambient O_3 (see also discussions by *Ridley et al.* [1988] and *Fehsenfeld et al.* [1990]). The magnitude of this potential artifact was <10% for NO_2

and <5% for NO for ambient O_3 mixing ratios of 100 and 200 ppbv at 0.15 and 6 km, respectively.

Other notable changes in the instrument from those previously reported include (1) the use of a common backward-facing sample inlet line with a baked-on porcelain glass coating, (2) automation of a serial gas standard dilution system based on mass flow controllers, (3) separate photon counting channels for each photomultiplier tube to extend linear dynamic range, (4) addition of a third sampling system for NO_y, and (5) a 40% reduction in the overall system size, weight, and electrical power requirements. The new common inlet system constructed from porcelain glass lined tubing exhibited less memory than PFA Teflon in simultaneous flow line tests conducted during the ABLE 3A test flights. The sample inlet line and photolytic cells were also thermally insulated.

The NO_y catalytic convertor system was adapted from that described by *Bollinger et al.* [1983], *Fahey et al.* [1985], and *Murphy and Fahey* [1987]. The convertor consisted of 35 cm long × 4.6 mm ID gold tubes operated at 300°C. CO was added as a reducing agent at a final mixing ratio of 3 parts per thousand (ppt). In order to reduce the residence time through the NO_y-LIF sample cell to a value of <5.0 s, four gold tubes were operated in parallel. Air samples were taken from the center of the common sampling line, through a short (<0.3 m) inlet, with a residence time of 0.4 s to the NO_y convertors. NO_2 was used to monitor NO_y conversion efficiency. Cleaning of the converter tubes, when necessary, was accomplished via the procedures described by *Fahey et al.* [1985]. NO_2 conversion efficiency was maintained at 98 ± 4% efficiency throughout the ABLE 3A field program.

To date, no interference has been identified in the TP/LIF measurement of NO, and interferences are believed to be ≤ ±2 pptv based upon nighttime measurements of NO mixing ratios at or below the limit of detection. The NO_2 photolytic convertor was operated with a wavelength >350 nm. This cutoff wavelength was selected to minimize potential interference from the photolysis of NO_x-containing organic compounds. The thermal decomposition of HO_2NO_2 and N_2O_5 yielding NO_2 may represent a potential interference in the measurement of NO_2 under cold high-altitude conditions, where these compounds have been predicted to have mixing ratios on the order of that of NO_2 [*Logan et al.*, 1981]. Attempts to quantify the magnitude of this potential interference are not yet definitive [*Gregory et al.*, 1990*a*; *Sandholm et al.*, 1990; *Ridley et al.*, 1989]. If HO_2NO_2 and/or N_2O_5 decomposition took place in these short residence time, thermostated photolytic convertor systems, then it has likely taken place heterogeneously through reactions on the inlet and cell walls, not through homogenous decomposition in the gas phase. In this case, the magnitude of the interference would be relatively insensitive to modest variations (twofold to threefold) in sample flow rate (an often used test for possible interferences). Final resolution of any potential problem arising from the decomposition of unstable NO_2-containing compounds requires further study. Until these issues can be more clearly discriminated, the NO_2 measurements presented here may need to be considered as upper limits under some sampling conditions (e.g., cold high altitude, and plumes rich in labile or photolytically active NO_x-containing compounds). It should be noted, however, that the NO_x/NO_y and NO_x/PAN ratios reported here and in a companion paper by *Singh et al.* [this issue (*a*)] represent some of the smallest free tropospheric values measured to date with the smallest ratios observed at the higher (i.e., colder) altitudes.

The TP/LIF sensor continuously measured the small background signal generated by the 226-nm laser beam, by tuning the laser wavelength off of the NO $X^2\Pi \rightarrow A^2\Sigma$ transition, and by blocking of the IR laser beam. This dominant background component of the instrument was subtracted for all measurements. Ambient nighttime clean air measurements made with our instruments yielded NO mixing ratios below, or at, the instrumental limit of detection. These nighttime values were often smaller than those measured from sampling zero-grade air gas cylinders. Similarly, mixing ratios of NO and NO_2 measured in "clean" ambient air have been less than those measured in air from cylinders. In the case of NO_y, a combination of chemical scrubbers has often reduced the mixing ratios of NO_y measured from zero-grade air cylinders by factors of twofold to fourfold. Based on these observations, the data set presented here has not been altered by the NO, NO_2, and NO_y concentrations measured in the gas streams produced from zero-grade air gas cylinders and associated flow line hardware (where in these ground tests ~20 m of additional flow line was added to the system). These results suggest possible systematic differences of approximately 4 ± 4 pptv for NO, 8 ± 8 pptv for NO_2, and 60 ± 60 pptv for NO_y could exist between the data reported here and other data sets in which zero-grade air NO, NO_2, and NO_y "blank" values were subtracted from ambient air measurements unless some other collaborating background measurement has been made (e.g., the routine measurement of nighttime NO mixing ratios not influenced by local sources). The chemiluminescence-based NO, NO_2, and NO_y measurements made at the ABLE 3A ground site were also not corrected for zero-grade air "blanks." These NO_x and NO_y measurements were in good agreement when extrapolated to those made on board the aircraft. However, small (0–4 pptv) differences in NO were incapable of being discerned even though an offset of about +2 pptv was reported for the ground-based data [*Bakwin et al.*, this issue].

Limits-of-detections (LOD's) for signal to noise ratios of 2/1 averaged 3.0 ± 1.5 pptv for NO and 8 ± 3 pptv for NO_2. Both LOD's had signal integration times of 3 min for data taken between July 8, and August 10, 1988. A slight increase in background noise counts was experienced in these earlier flights. This problem was corrected and resulted in improving the LOD's for the remainder of the program (August 11–17, 1988) to 1.4 ± 0.4 and 5 ± 2 pptv for NO and NO_2, respectively. The absolute accuracy of the calibration transfer to the NO and NO_2 measurements was estimated at the 95% confidence limit at ±16% and ±18%, respectively [cf. *Gregory et al.*, 1990*a*, *b*]. The NO_y measurements were consistently above the detection limit and typically exhibited a measurement precision (at the 95% confidence limit) of ±8.5% and ±15% at 700 and 200 pptv, respectively. NO and NO_y data were reported for 1-min integration times. NO_2 data were reported using either 3- or 6-min signal integration time periods.

3. Overview of Flights and Conditions

There were 33 aircraft missions conducted during the ABLE 3A program. The first five missions constituted the

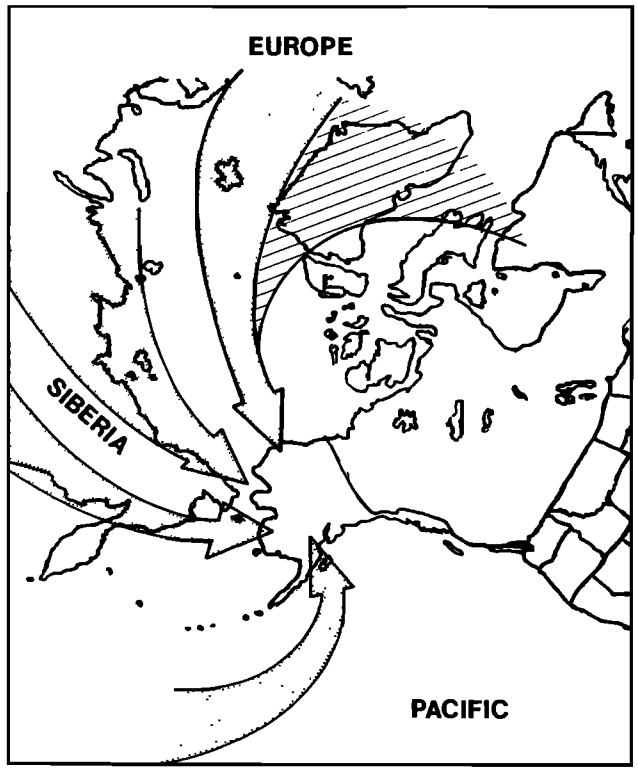

Fig. 1. Major pathways for medium- to long-range air mass transport to Alaska.

transit from Wallops Island, Virginia → Thunder Bay, Canada → Churchill, Canada → Thule, Greenland → Fairbanks, Alaska → Barrow, Alaska, over the period July 7–10, 1988. These missions predominantly occurred in the middle free troposphere from 4.5 to 6.1 km. An altitude of 6.1 km represented the ceiling limit of the Wallops Flight Facility L-188 Electra with the ABLE 3A payload. The next seven missions (6–12) were based out of Barrow, Alaska, and covered the time period from July 12 to July 21, 1988. After a transit flight from Barrow to Bethel, Alaska, on July 24, 1988, eight more missions (14–21) were conducted from Bethel during the period July 26 to August 4, 1988. Following this, three missions (22–24) were dedicated to measuring trace gas distributions over the northern edge of the Pacific Ocean with an excursion to Cold Bay in the Aleutian Islands from August 7 to 8, 1988. Two additional missions (25 and 26) were conducted out of Bethel on August 9–12, 1988. The flight program concluded with seven transit flights (27–33 from August 11–17, 1988) from Bethel, Alaska → Barrow, Alaska → Thule, Greenland ← → Alert, Thule → Frobisher Bay, Canada → Goose Bay, Canada → Portland, Maine → Wallops Island, Virginia. There were four primary measurement goals for these missions: (1) midtropospheric spatial distribution (primarily transit flights), (2) boundary layer composition, (3) flux measurements, and (4) vertical distributions. A more detailed description of the mission profiles and individual mission objectives are contained in the ABLE 3A overview paper [*Harriss et al.*, this issue (*a*)].

The dominant air mass source regions encountered during the ABLE 3A missions are represented in Figure 1. This general representation was derived from the trajectory analyses of *Shipham et al.* [this issue] and the GTE/ABLE 3A data archive. Air mass trajectory analyses, synopses of meteorological conditions, and potential vorticity contours contained in this paper were derived from the analyses of *Shipham et al.* [this issue] and the ABLE 3A archive.

The summer of 1988 was somewhat warmer and drier than the climatological mean for the Bethel region, especially early in the season, whereas conditions at Barrow were close to the norm. During the ABLE 3A program, the air mass back trajectories over the Barrow region correlated reasonably well those of with the 5-year climatology reported by *Miller* [1981]. Notable, however, was an apparent lack of trajectories originating from the south to southwest (specified as sectors 22 and 23 in Figure 1 of Miller's paper). These sectors represented a sizable percentage (~30–40%) of the 5-year climatology of July average air mass trajectory origins for the Barrow region. Air masses encountered near Barrow that originated from these sectors were only sampled on portions of missions 6 and 7. Air masses sampled over the Bethel region, however, had a large fraction of trajectories that originated from the south to southwest. Overall, the "snap-shot" view of the troposphere sampled over Alaska for the entire ABLE 3A program appears to represent somewhat typical conditions, as we sampled proportionally from all of the major air mass origin sectors for the region.

4. Observations and Discussion

During the ABLE 3A program, the middle/lower tropospheric column over Alaska was frequently stratified. This stratification suggests that the different air masses sampled could have been derived from a variety of source regions. Haze layers were encountered on several missions, and these layers were often apparent in the lidar aerosol data at altitudes from the mixed layer to the tropopause. *Brock et al.* [1989] observed similar discrete haze layers within the summertime middle troposphere over the high-latitude regions of North America and Greenland. They described particular haze layers, which were depleted in both O_3 and odd nitrogen containing compounds (as measured by a luminol instrument) relative to adjacent air, which contained fewer particles. In these cases, an enhancement in the concentration of nucleation mode particles (<0.1 μm) was also observed within the haze layer along with significant enhancements of new particle production at the layer's boundary. Their findings suggested that these haze layers were probably derived from anthropogenic or biomass burning sources, or both. Based upon their observations and those made during the ABLE 3A program, the occurrence of haze layers appears to be a common phenomenon within the summertime middle troposphere over high northern latitudes.

During July and August, numerous "forest" fires were reported throughout most of Alaska lying south of the Brooks Range (see also discussion by *Shipham et al.* [this issue]). On several occasions, biomass burning emissions produced enhancements in aerosol number density and in the mixing ratios of numerous trace gases. These enhancements were encountered in the form of well-defined haze layers and localized entrapment within the mixed layer. Several discrete haze layers encountered during the ABLE 3A program (on missions 14, 20/21, and 23) have been analyzed for their chemical signatures in the companion paper of *Wofsy et al.* [this issue]. The haze layers sampled on

missions 14 and 20/21 have been described as modestly aged (a few days) plumes generated from biomass burning emissions that occurred within the Kuskokwim Delta region of Alaska. In contrast, the haze layer sampled on mission 23 possessed a chemical signature that suggested long-range transport from anthropogenic source regions.

Browell et al. [this issue] have used nadir and zenith lidar aerosol-scattering measurements to obtain an estimate of the fraction of the tropospheric air masses that contained distinct haze layers. Their estimates suggest about 10% of the lower 4-km tropospheric column overflown during the ABLE 3A program contained discrete haze layers. They also estimated the 4- to 6-km region contained 1–4%, and the 6- to 8-km region 1–2%. In addition, Browell et al. estimated the fraction of high-latitude "background" air and air of suspected stratospheric origin. They described high-latitude background air as having O_3 mixing ratios in the range of 25–35 ppbv just above the mixed layer (0.5–2 km) that increased in proportion to altitude by 5.5–7.5 ppbv/km. Using this characterization, they estimated that of the encountered air masses, background air was observed about 35% of the time in the 2- to 4-km region and about 50% for both the 4- to 6-km and the 6- to 8-km regions. Characterization of air masses of suspected stratospheric origin was based on O_3 mixing ratios larger than values found in background air with coincident small values of aerosol scattering. Air of stratospheric origin was estimated to have been encountered about 35%, 50%, and 50% of the time for the 2- to 4-km, 4- to 6-km, and 6- to 8-km altitude regions, respectively. These estimates only apply to the air masses overflow, and their measurements were limited to cloud-free conditions.

Several scientific issues merit clarification prior to our use of these classifications for assessing factors controlling the abundance of reactive odd nitrogen. In particular, air sampled during this program that was characterized as originating from the stratosphere usually contained mixing ratios of H_2O that are more typical of the middle/upper troposphere (i.e., $\gg$15 ppmv). In addition, the representativeness of the carefully characterized haze layers derived from Kuskokwim Delta biomass burning emissions should be addressed prior to extrapolating emission factors to the majority of Alaskan or other sub-Arctic fire emissions. In order to further define the possible impact of haze layers and stratospheric/tropospheric exchange on the reactive odd nitrogen budget within the middle/lower tropospheric column (<6 km) over Alaska, several case studies warrant discussion below.

4.1. *Case Studies*

4.1.1. *Case study mission 6.* The air mass sampled near Barrow, Alaska, during mission 6 (on July 12–13, 1988) contained strata that could be characterized as haze layers, air of stratospheric origin, and background air based upon the previous descriptions. Plates 1 and 2 illustrate the lidar soundings of relative aerosol scattering and O_3 mixing ratios measured along a portion of a 6.1-km flight leg during this mission (6). The region between about 4.8 and 5.5 km produced small values of relative aerosol scattering in the near-infrared spectral region (IR = 1.06 μm). These values fell within the range of values used to describe air of stratospheric origin. In addition, O_3 mixing ratios within this air parcel were enhanced (i.e., O_3 > 70 ppbv) compared to mixing ratios in background air. The region near 3 km appeared to consist primarily of background air. Enhanced values of relative aerosol scattering in the visible wavelength spectral region were observed between 7 and 8 km (zenith IR lidar not operational on this mission). This haze layer extended down to the aircraft altitude and was sporadically sampled along with aerosol-depleted/O_3-rich air parcels, during both the 6.1-km flight leg and the spiral descent made near point A (as depicted in Plate 1). The vertical soundings produced from in situ measurements of CO, O_3, relative humidity (% RH), and NO_y taken during this descent are illustrated in Figure 2. Vertical soundings of the hydrocarbons C_2H_2, C_2H_6, and C_3H_8 are presented in the companion paper of *Blake et al.* [this issue].

Several meteorological factors contributed to the characteristics of the midtropospheric air mass sampled on this mission. High pressure persisted over central and northern Alaska at the 500-mbar level for several days prior to the flight (July 9–11, 1988). During this period, regions of low pressure were centered over western Siberia and the Gulf of Alaska. The high pressure over Alaska migrated to the Queen Elizabeth Islands from July 11 to 13, 1988, while a broad area of low pressure developed off the northeastern coast of Siberia. This resulted in a southerly flow of air along the high-pressure ridge that extended north through most of western Alaska. Calculated values of Ertel potential vorticity (Epv) at the 500-mbar pressure level exceeded the nominal threshold values often associated with air of stratospheric origin (Epv $\geq 1 \times 10^{-5}$ K hPa^{-1} s^{-1}) in areas near the Gulf of Alaska low and a strong low-pressure system north of the Aleutians (183°W, 55°N). These regions of enhanced potential vorticity covered areas of about 2–4 $\times$ 10^5 km^2 and were centered near the indicated origin of the sampled air mass (151°W, 51°N on July 8 and near 178°W, 49°N on July 10–11). Three-day isentropic back trajectories along the Θ = 310°K potential temperature surface (~500 mbar) indicated an almost due north flow of air along the high-pressure ridge. These trajectories indicated the air mass originated near 168°W, 57°N at the northern end of the Aleutians between the two low-pressure systems on July 10, 1988. These back trajectories also crossed regions where several large fires were burning in the southwestern foothills of the Brooks Range (near 160°W, 66°W) about 24–32 hours prior to reaching the Barrow area (see *Shipham et al.* [this issue] for fire locations).

Given these conditions, it may be reasonable to tentatively assign the origin of the encountered haze layers to fires burning in the southwestern foothills of the Brooks Range. The mechanism responsible for transport of the portion of the air mass (air parcel) suspected to have been of stratospheric origin is currently less clear. Several mechanisms, consistent with the meteorological conditions, offer possible explanations: (1) the air parcel was a remnant of a cutoff region formed in association with the Gulf of Alaska low, (2) the air parcel was influenced by jet streak activity on the southern edge of the Bering Sea low, or (3) the air parcel was produced by downward transport of upper tropospheric/lower stratospheric air following tropopause relocation. Due to the mixing in of tropospheric air, all of these mechanisms could result in air parcels with chemical signatures significantly modified from those characteristic of stratospheric air.

A similar example of O_3-enhanced air was found during mission 18 (on July 31, 1988) near Bethel. In this case,

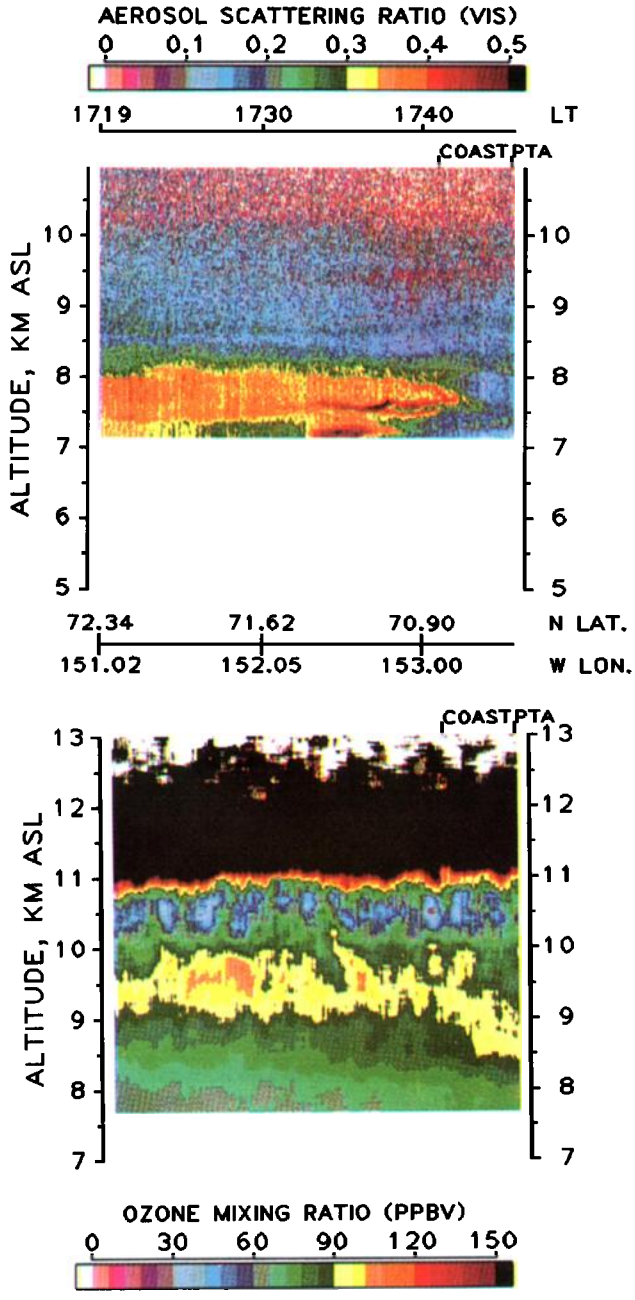

Plate 1. Aerosol and O_3 distribution measurements made on July 12, 1988, during mission 6. The zenith airborne differential absorption lidar (DIAL) aerosol (top panel) and O_3 (bottom panel) data are shown in false color display with the relative amount of atmospheric back scattering and O_3 mixing ratio in parts per billion by volume (ppbv) defined at the top or bottom of the respective displays. In either case, black represents values greater than the maximum given on the color scale. The altitude is in kilometers above sea level (ASL). Local time is at the top of the aerosol display, and the aircraft latitude and longitude information is given in degrees at the top of the O_3 display.

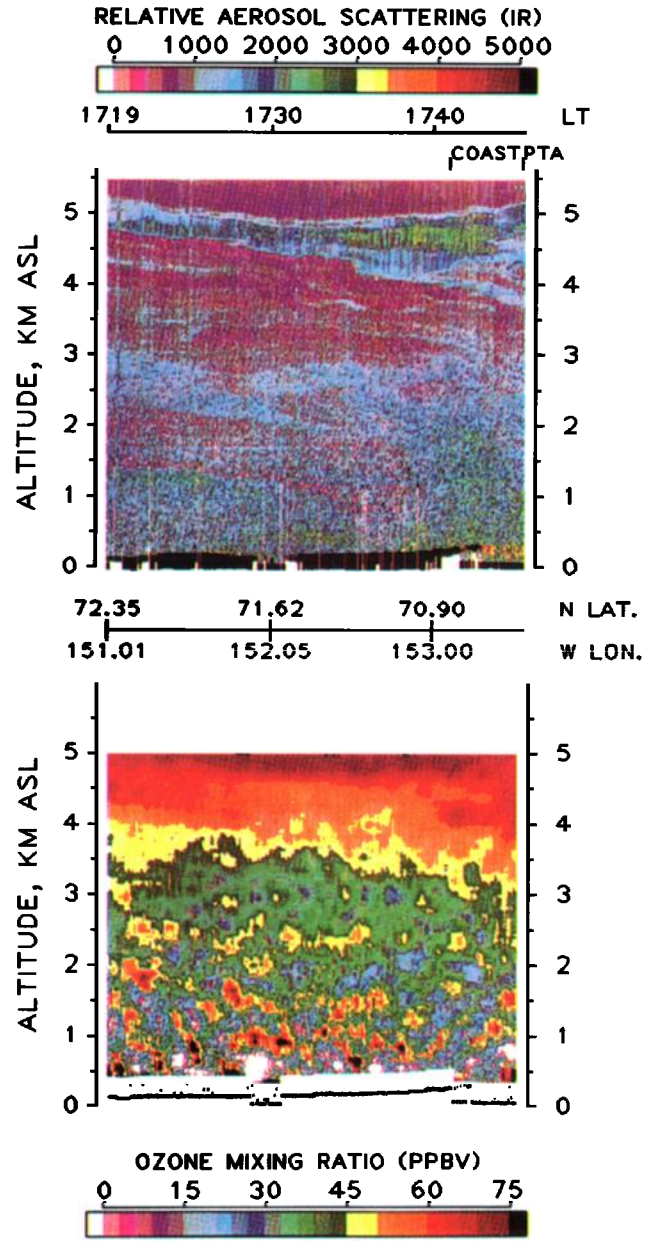

Plate 2. Nadir aerosol and O_3 distributions obtained by the airborne DIAL system on July 12, 1988, at the same time as the zenith data presented in Plate 1.

however, the O_3-enhanced region appeared in the form of a distended tropopause rather than a more well-defined O_3-enhanced stratum (cf. Plate 3). Back trajectory analysis also indicated that movement of this air parcel was controlled by a ridge of high pressure, which had built up along a line from Norton Sound to Anchorage, concurrent with a low-pressure system over the Aleutians and a strong Polar low located north of Prudoe Bay. Calculated Epv values were larger than the stratospheric threshold value in the vicinity of the Aleutian low, near the region where this air mass appears to have originated. A complete meteorological analysis (in progress), capable of providing a detailed characterization of mechanisms affecting these and other ABLE 3A case studies, is beyond the scope of this paper and will be presented in a subsequent paper(s).

The ratio NO_y/O_3 had a value of about 0.12 for air suspected of having a stratospheric origin, which was encountered sporadically along the 6.1-km flight leg of mission 6. This NO_y/O_3 ratio was larger than ratios expected from high-latitude middle-stratospheric air (~0.005 [*Murphy et al.*, 1992]). This larger ratio could suggest a large fraction (~50%) of the NO_y abundance within the depleted-aerosol/enhanced-O_3 air parcel may have originated from sources

other than the stratosphere, unless significant air mass aging resulted in an increased loss of O_3 relative to NO_y during the downward transport of this air from altitudes well above the tropopause (i.e., >4 km above the tropopause).

Several compounds exhibited enhancements, which correlated with those of CO, within the haze layers on mission 6. Enhancement factors relative to CO (i.e., $\Delta M/\Delta CO$) for these layers differed somewhat from those characterized for several of the other haze layers encountered during the ABLE 3A program [*Wofsy et al.*, this issue]. The enhancement factor $\Delta NO_y/\Delta CO$ extrapolated from the 6.1-km flight leg portion of mission 6, where mixing ratios of NO_y reached a maximum (1.9 ppbv), yielded a $\Delta NO_y/\Delta CO$ of about 0.025 (±0.01). For the chemically enhanced layers encountered near 5.0 and 4.3 km during the spiral descent, $\Delta NO_y/\Delta CO$ was approximately 0.015 (±0.005). These enhancement factors were larger than the 0.003–0.008 range of values reported for two layers produced from biomass burning within the Kuskokwim Delta region, and are closer to enhancement factors reported for biomass burning in other regions [see *Wofsy et al.*, this issue]. Enhancement factors for C_2H_6 and C_3H_8 relative to CO also differed from those found in the haze layers over the Kuskokwim Delta. However, the mixing ratios of these hydrocarbon compounds and CO found outside of the haze layer on mission 6 did fall within the range characterized as typical for background high-latitude air observed during the ABLE 3A program [*Blake et al.*, this issue]. These larger enhancement factors may have resulted from differences in the ecosystem types burnt (e.g., taiga versus tundra/Boreal forest), or the ecosystem ages, or the ages of the plumes, or a combination of all these factors. This suggests that a larger range of enhancement factors might be implied for high-latitude haze layers produced by biomass burning than the limited range found over the Kuskokwim Delta region.

The thin O_3-depleted stratum occurring near 10–10.5 km (Plate 1) was observed on several occasions. This type of layer was usually observed just below, or in association with, a thin layer of enhanced aerosol scattering. These strata predominantly occurred within about 1 km of a generally well-defined (via measured O_3 profile) tropopause. This trend was also observed over high-latitude regions of Canada during the ABLE 3B program (July/August 1990). On several occasions during the ABLE 3B program, portions of this type of stratum were believed to have been sampled following these air parcels' downward transport into the middle troposphere. NO_y was found to be enhanced by about 1.5- to 2-fold within these O_3-depleted air parcels, whereas CO mixing ratios were near background values (R. W. Talbot et al., Summertime distribution and relations of reactive nitrogen species and NO_y in the troposphere over Canada, submitted to *Journal of Geophysical Research*, 1992). The origin of these air parcels remains a mystery, although there was some indication (as is the case shown here for mission 6) that advection from high-altitude air traffic corridors may have been important. The chemical characteristics of these O_3-depleted strata certainly merit future investigation.

4.1.2. *Case study mission 12.* The air mass sampled near Barrow during mission 12 (on July 21–22, 1988) also contained an air parcel of suspected stratospheric origin, characterized by small values of aerosol scattering and enhanced O_3 mixing ratios (cf. Plate 4). Three-day isentropic

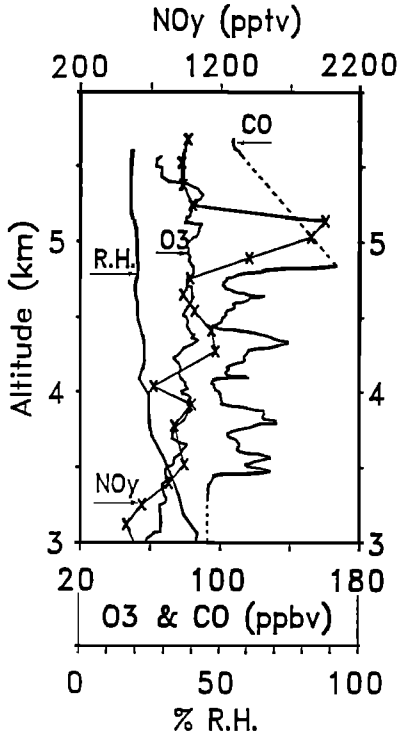

Fig. 2. Vertical sounding taken near Barrow, Alaska, during mission 6 (70.3°N, 153.7°W) on July 12, 1988, where O_3, CO, relative humidity (% RH), and NO_y (crosses) are shown as a function of altitude.

back trajectory analyses along the Θ = 310 K potential temperature surface (~500 mbar) indicated northerly air flow extending to about 83°N. Past this point, two possible air mass origins were indicated: the Taymyr Peninsula and the Queen Elizabeth Islands. Analyses along the Θ = 300 K surface (~625 mbar) followed a similar path but only toward the Queen Elizabeth Islands. As in mission 6, calculated values of Epv (at the 500-mbar level) exceeded the threshold value for stratospheric air in the vicinity of both of the indicated air mass origins (i.e., the Taymyr Peninsula and the northern end of Baffin Bay, 75°W, 75°N). Although certainly not conclusive, this tends to support the speculation that the 4-km air parcel was of stratospheric origin.

Figure 3 illustrates the vertical soundings obtained from the in situ measurements of CO, O_3, NO_y, and relative humidity (% RH) made during a spiral descent near 156.8°W, 72.2°N on mission 12. Extrapolation of the ratio $\Delta NO_y/\Delta O_3$ determined from the difference in mixing ratios between the O_3-enhanced air parcel near 4 km and the air sampled near 3 km yielded $\Delta NO_y/\Delta O_3 \sim 0.01$. This value was once again larger than that expected for stratospheric air. As in the mission 6 case study, the magnitude of the NO_y/O_3 ratio in conjunction with the general wetness of the air parcel suggests that this air parcel was modified with tropospheric air during its downward transport. Such chemical modification would have been necessary for this air parcel's origin to have been from regions well above the tropopause.

Mixing ratios of C_2H_2, C_2H_6, C_3H_8, and CO within the air parcels near 4 and 3 km were near or slightly smaller than values characterized as typical for high-latitude background air [*Blake et al.*, this issue]. This, in conjunction with the small NO_x mixing ratios (~20 pptv) measured in the air

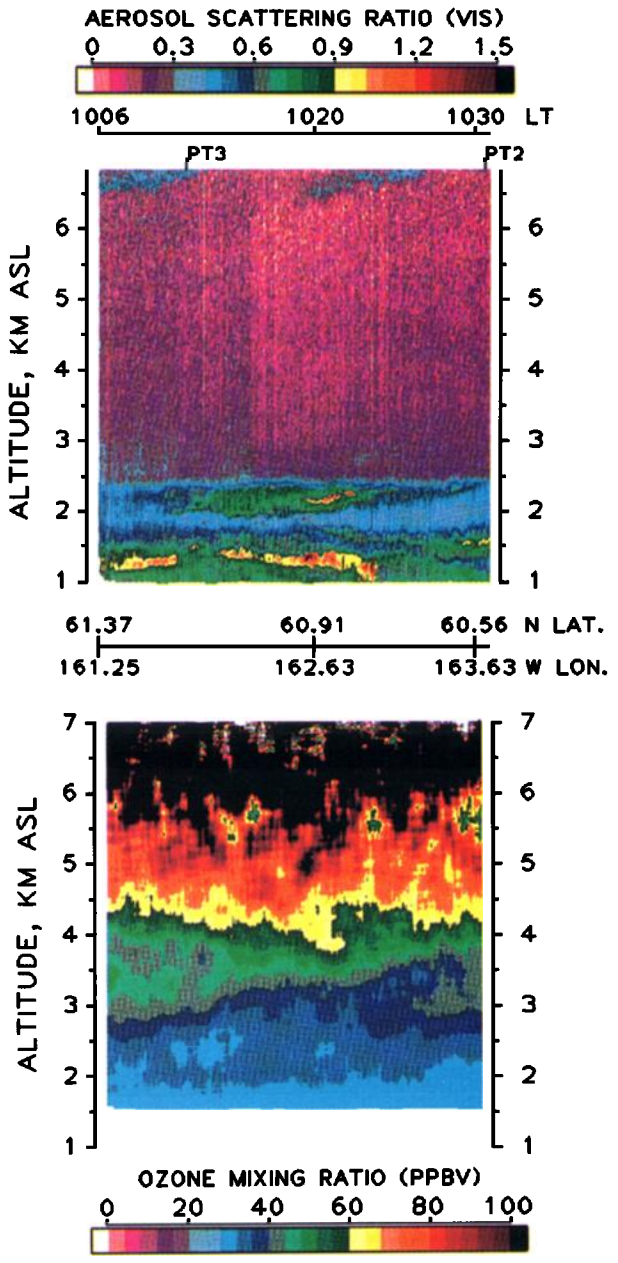

Plate 3. Nadir aerosol and O_3 distributions obtained on July 31, 1988, during mission 18.

parcel near 4 km, supports the argument that the enhancement in O_3 mixing ratios was not solely produced by recent net in situ photochemical production from pollution precursor compounds. Although modified, the O_3 enhancement within this air parcel appears to have been stratospherically derived.

4.1.3. *Case study mission 13.* The air mass sampled near Bethel, Alaska, during mission 13 (on July 24–25, 1988), also contained an air parcel of suspected stratospheric origin. This air parcel had a spatial appearance resembling a tongue of O_3-rich air that had formed into a horizontal layer near 2 km (cf. Plate 5). These soundings were made during a flight leg from Norton Sound to Bethel, where the growth in mixed layer height was quite apparent upon crossing the coast.

Five-day isentropic back trajectory analyses along the Θ = 300 K potential temperature surface indicated descending northerly air flow for the 3-day period prior to this mission (13). This flow pattern was preceded by cyclonic air flow around a strong Polar low during the fourth and fifth days prior to the mission. These trajectories indicated an air mass origin near 105°W, 75°N (at ~550 mbar, on July 20, 1988) that was transported to 162°W, 61°N (at ~700 mbar, on July 25, 1988). Calculated Epv values for the 500-mbar pressure level exceeded threshold values for stratospheric air, on July 21 and 23, 1988, near the center of the low located just west of Banks Island (at about 130°W, 74°N).

Figure 4 illustrates the vertical soundings obtained from the in situ measurements of CO, O_3, NO_y, and relative humidity made during a spiral descent near 161.9°W, 61.1°N. Mixing ratios of O_3 were larger than background values from 6.1 to 1.7 km, whereas mixing ratios of CO, C_2H_2, C_2H_6, and C_3H_8 were all near their median values described for background air. NO_y/O_3 ratios ranged from about 0.006 to 0.012 and were close to but still larger than ratios found in

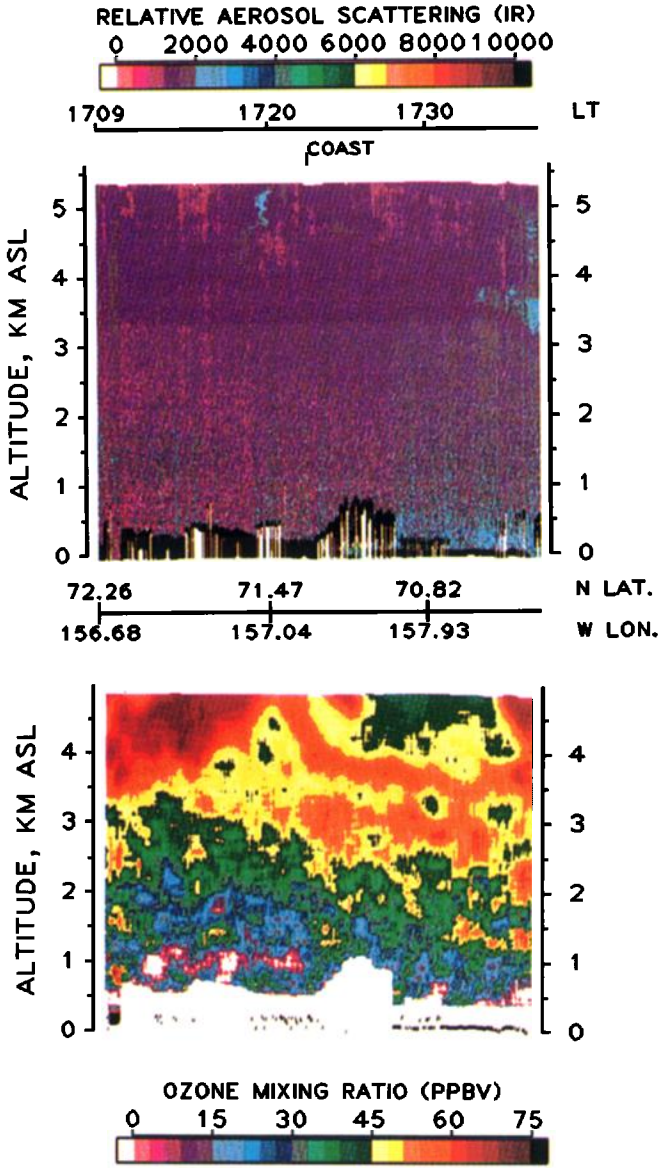

Plate 4. Nadir aerosol and O_3 distributions obtained on July 21, 1988, during mission 12.

stratospheric air. This, coupled with the general wetness of this air parcel, again suggests modification of this air, if it originated in the middle stratosphere.

4.1.4. *Case study mission 8.* During mission 8 (on July 15, 1988) an air parcel containing the largest mixing ratios of O_3 (~300 ppbv) measured (in situ) during the ABLE 3A program was encountered near 4.2 km at the northern end of a flight leg north of Barrow. The lidar O_3 soundings did not indicate a tongue of stratospheric air or other signs of stratospheric folding within the tropospheric column along this constant altitude flight leg. Even so, a tongue of stratospheric air originating outside of the flight track could not be ruled out as the source of this air parcel. Measured dew point values (≤ -42°C) within this air parcel were at or below the lower limit of the three-stage hygrometer being used, and could not provide an accurate assessment of the water vapor content within this air parcel. Thus, the contention that this air parcel was of stratospheric origin could not be supported by either lidar O_3 soundings or water vapor measurements.

Epv values calculated for the area north of Barrow were not larger than the threshold value for stratospheric air. However, calculated Epv values at the 400-mbar level were significantly larger (Epv ~5×10^{-5} K hPa^{-1} s^{-1}) than stratospheric threshold values at this air parcel's indicated origin, which was over the Taymyr Peninsula. The Epv values calculated for this region were close to those given by *Gidel and Shapiro* [1980] for lower stratospheric air with O_3 mixing ratios of ~300 ppbv. These large potential vorticity values were, however, not indicated to have been preserved along with O_3 during the 3-day transit of the air parcel encountered on mission 8 from the Taymyr Peninsula to the area north of Barrow. In this case, potential vorticity appeared to have had an apparent "lifetime" of about a day, whereas mixing ratios of O_3 and perhaps other compounds may have changed by only a small amount (except for possibly H_2O, which could have been significantly perturbed by even small (5–20%) contributions of tropospheric air containing 0.5–1.0 parts per thousand (pptv) H_2O).

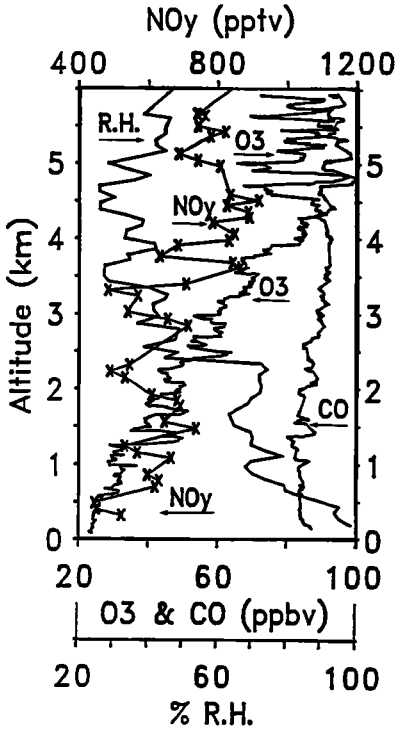

Fig. 3. Vertical sounding taken over the Arctic Ocean pack ice during mission 12 (72.2°N, 156.8°W) on July 22, 1988, where O_3, CO, relative humidity (% RH), and NO_y (crosses) are shown as a function of altitude.

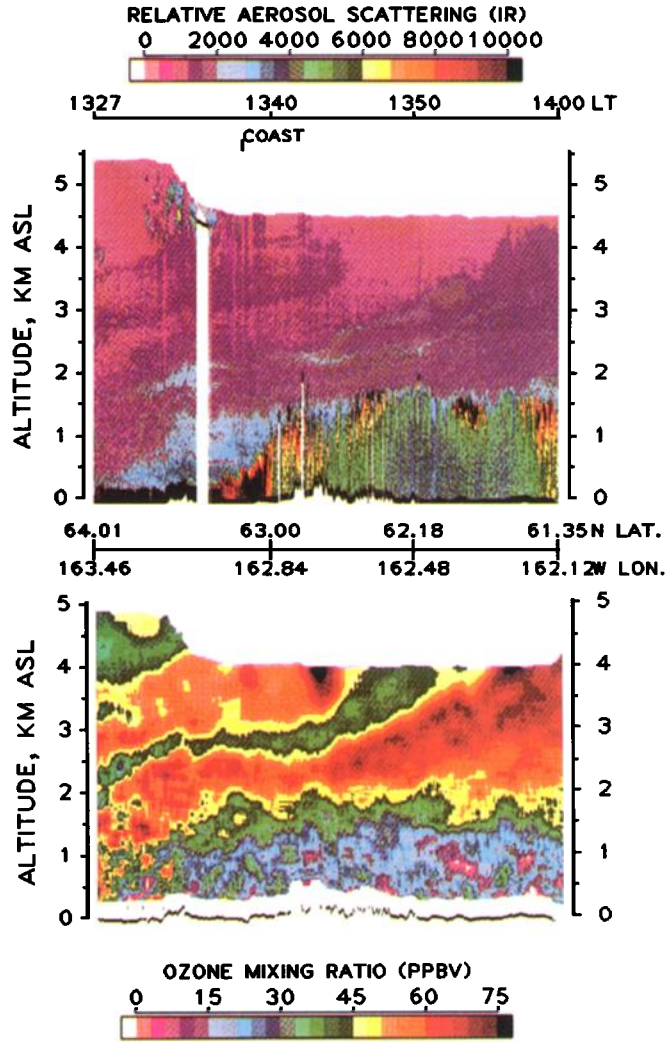

Plate 5. Nadir aerosol and O_3 distributions obtained on July 24, 1988, during mission 13.

In situ measurements of CO and CH_4 also suggested this air parcel was aged with respect to typical mid-latitude tropospheric conditions. Mixing ratios of both CO and CH_4 were the smallest measured during the program (CO ~60 ppbv, and CH_4 ~1652 ppbv). These mixing ratios were about 35 and 45 ppbv smaller than those measured in air adjacent to the O_3-enhanced air parcel. CO mixing ratios near 60 ppbv are close to those given by *Warnek* [1988] for the northern hemisphere's lower stratosphere, but are about twofold larger than those found by *Murphy et al.* [1992] for stratospheric air containing ~300 ppbv O_3 over Darwin, Australia. This difference most likely reflects the interhemispheric gradient in background CO mixing ratios of approximately 30–40 ppbv. The small CO and CH_4 mixing ratios found in this northern hemispheric air parcel support the contention that this O_3-enhanced air parcel originated from the lower stratosphere.

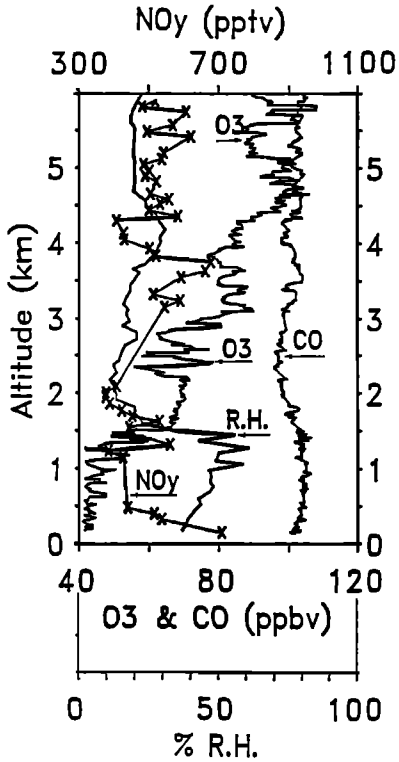

Fig. 4. Vertical sounding near Bethel, Alaska, during mission 13 (61.1°N, 161.8°W) on July 24, 1988, where O_3, CO, relative humidity (% RH), and NO_y (crosses) are shown as a function of altitude.

Values of the ratio $\Delta NO_y/\Delta O_3$ (0.0010 ± 0.0003) were calculated using the differences in mixing ratio values measured in the center of the O_3-enhanced air parcel with air adjacent to it. These values were consistent with NO_y/O_3 ratios measured by *Kondo et al.* [1990] within the stratosphere near the tropopause (NO_y/O_3 ~0.0015 ± 0.0005 for altitudes <16 km), but are significantly smaller than values (~0.005) found near Stavanger, Norway [*Murphy et al.*, 1992]. The value of the ratio NO_y/O_3 within the air parcel encountered on mission 8 (~0.002) was also within the range of NO_y/O_3 ratios observed in the middle/lower stratosphere by Kondo et al., but smaller than the values of Murphy et al. The small values of $\Delta NO_y/\Delta O_3$ and NO_y/O_3 measured in the event on mission 8 could represent relatively rapid loss of NO_y if scavenging processes had affected the large HNO_3 fraction of NO_y expected to be present in stratospheric air (HNO_3 ~ 75% of NO_y [e.g., *Russell et al.*, 1988]). If HNO_3 was almost completely lost from this air parcel, resulting in a 75% reduction in NO_y, then the measured $\Delta NO_y/\Delta O_3$ and NO_y/O_3 ratios could be extrapolated to the values summarized by Murphy et al. Alternatively, if HNO_3 was not lost during transport from the lower stratosphere, then these results might imply smaller NO_y/O_3 ratios for the summer high-latitude lower stratosphere than those found in the fall/winter/spring by *Murphy et al.* [1992]. Unfortunately, due to the long sampling time of the HNO_3 instrument used in ABLE 3A, the HNO_3 fraction of NO_y could not be evaluated for this event.

4.1.5. *Additional case studies.*

Inputs of upper tropospheric/lower stratospheric air: O_3-enhanced air parcels with small values of aerosol scattering were also encountered on missions 7, 11, 14, 15, 16, 18, 19, 24, and 25. Lidar aerosol and O_3 soundings made on missions 7, 15, 19, and 23 have been presented by *Browell et al.* [this issue]. Tongues of stratospheric air associated with tropopause folding were encountered (most notably on missions 19 and 30 [*Browell et al.*, this issue]), whereas the mechanisms responsible for other events were not obvious. As mentioned earlier, several possible mechanisms resulting in downward transport of upper tropospheric/lower stratospheric air could account for the composition of these O_3-enhanced air parcels. In most of these cases, calculated values of Epv exceeded the stratospheric threshold value along their 3- to 5-day isentropic back trajectory paths. Figure 5 presents the frequency distribution of the occurrence of Epv values larger than the stratospheric threshold at the 500-mbar pressure level during July and August 1988. In

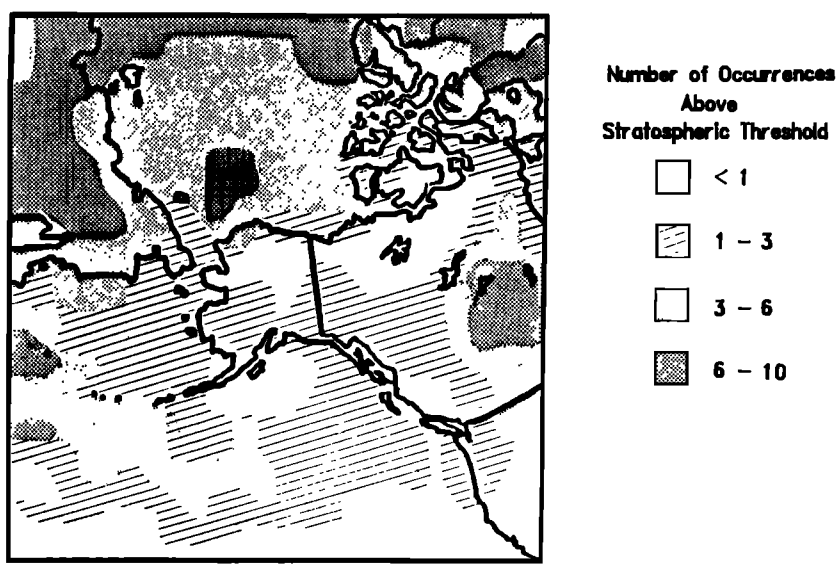

Fig. 5. Probability density plot for Ertel potential vorticity exceeding the stratospheric threshold value over the Arctic during July and August 1988.

general, these events appeared to have covered spatial scales of the order of 10^5 km^2. Most of the active areas shown in Figure 5 lie within the range of 3- to 5-day back trajectories from Alaska. These areas also exhibited a larger frequency of occurrence (i.e., stronger activity) near northern Siberia during July, and near Greenland during August. This shift followed the eastward migration of the strong Polar low.

Although admittedly circumstantial, these cases do support the idea of significant downward transport into the middle/lower troposphere over Alaska of air that resided within the vicinity of the tropopause (tropopausal air). The NO_y/O_3 ratios measured within the air parcels of this type fell within the range of values found for the case studies discussed in detail (i.e., $NO_y/O_3 \sim 0.009 \pm 0.005$). The values of $\Delta NO_y/\Delta O_3$ extrapolated from measurements taken within and adjacent to these air parcels also fell within those given in the case studies (i.e., $\Delta NO_y/\Delta O_3 \sim 0.007 \pm 0.005$). In general, these values are all larger than those expected for lower stratospheric air and suggest a large fraction of the NO_y may have originated from nonstratospheric sources (e.g., lightning and high-altitude aircraft [cf. *Murphy et al.*, 1992; *Ehhalt et al.*, 1992]).

Inputs from anthropogenic sources: Relatively fresh (<1 day) anthropogenically produced emissions were encountered, but only rarely. Plumes from small villages and the downwind plumes from Bethel and Barrow were encountered on occasion. These sources are believed to contribute negligibly to the regional budgets of NO_x, NO_y, CO, or NMHC's, although mixing ratios very near the source (<20 km) were as much as 1.5-fold larger than background air values within the mixed layer. Emissions from petroleum industry activity at Prudoe Bay apparently enhanced free tropospheric NMHC mixing ratios to the northeast of this area and were the only important source of fresh anthropogenic perturbations found in the free troposphere over the areas studied [*Blake et al.*, this issue]. Unfortunately, these encounters occurred either very early or late in these flights, during periods when the various N_xO_y instruments were in warm-up or shut-down cycles.

Enhanced mixing ratios of NO_x and NO_y were measured over about a 100-km region of the northern Pacific Ocean within the marine boundary layer (altitude ~0.15 km) during mission 23 (on August 7, 1988). NO_y mixing ratios (~700 pptv) in the center of the plume were about 2.5-fold larger than those measured in air adjacent to the plume. The enhancement in NO_x mixing ratios (~15 versus ~270 pptv) accounted for about 65% of the peak enhancement in NO_y that was observed about 40 km downwind from two cargo ships traveling westward along the shipping lane lying south of the Aleutians. This case is of interest, as ship traffic uses a few percent of the world's annual fossil fuel consumption [*National Academy of Sciences*, 1980]. In addition, global ship traffic is increasing at a rate of about 8% per year, and continued growth is projected with the globalization of world markets [*U.S. Department of Transportation*, 1988].

Shipping lanes still, for the most part, follow fairly narrow corridors along trade wind routes. Within these corridors, ship trails (plumes) can remain relatively well defined over distances of several hundred kilometers [*Porch et al.*, 1990]. The anthropogenic emissions from these multimegawatt (tens to hundreds of megawatts) mobile power plants may provide a locally potent source of NO_x to remote and otherwise pristine oceanic regions. These sources could also inject a significant burden of NO_x directly into the trade winds, especially at night. This large NO_x/NO_y fraction could then be converted to HNO_3 above the marine mixed layer, in a region with possibly less HNO_3 loss due to deposition. This mechanism of NO_x transport and transformation may explain at least a portion of the apparently anomalous Mauna Loa data treated by *Levy and Moxim* [1989] and *Moxim* [1990]. Active shipping lanes exist along the isentropic and three-dimensional trajectory paths they examined. The NO_x/NO_y enhancements measured off the Aleutians suggest that the world's ocean surface should not necessarily be treated as a vast, sourceless region for N_xO_y compounds.

Mixing ratios of CO were not significantly enhanced in the ship plumes encountered on mission 23 (G. W. Sachse, private communication, 1990) and followed a similar trend of large $\Delta NO_y/\Delta CO$ enhancement factors (i.e., small CO production) observed in other shipping lanes and in high-altitude aircraft corridors. These relationships emphasize the efficient combustion nature of these high-temperature NO_x sources. Thus, deconvoluting the influence of these sources on the remote troposphere may require careful examination of nonstandard combustion tracers.

4.2. *Composite Chemical Characterization of the Lower 6-km Column Over Alaska*

Presented in this section are composites taken from 26 vertical soundings made over Alaska in the form of slow rate-of-ascent/descent spirals (75–150 m/min). Location, day, and time for each individual sounding are given in the companion paper of *Blake et al.* [this issue]. Air mass back trajectory analyses and meteorological conditions for each mission are given in the companion paper of *Shipham et al.* [this issue]. The composites were generated by combining data bases from multiple flights and "binning" each chemical or meteorological variable's values among 10 bins equally covering the range of values measured for that variable. The binned concentration data were then broken out into four altitude regions centered at 0.75, 2.25, 3.75, and 5.3 km, which cover the altitude ranges of 0.15–1.5 km, 1.5–3.0 km, 3.0–4.5 km, and 4.5–6.1 km, respectively. These data are presented in pseudo-three-dimensional form, where the z axis represents the fraction of measurements occurring within a particular mixing ratio bin for each altitude range (Figures 6, 8, and 11). The base data set for these composites was generated by averaging temporarily overlapped measurements of other chemical/meteorological variables into a 3-min time base consistent with the NO_x-NO_y measurements. These composites used all of the measurements made during each sounding, including chemically enhanced regions or layers.

All constant altitude flight legs were, however, excluded from this analysis. In addition, four soundings were excluded from the analyses because they represented duplicates, containing nearly identical vertical structure information as soundings used within the same air mass. The rationale for these exclusions was based on creating composites that would not be overly biased by any one day's events or a particular sampling altitude.

4.2.1. *Distribution of odd nitrogen compounds and O_3*. Figure 6 illustrates the vertical composites for mixing

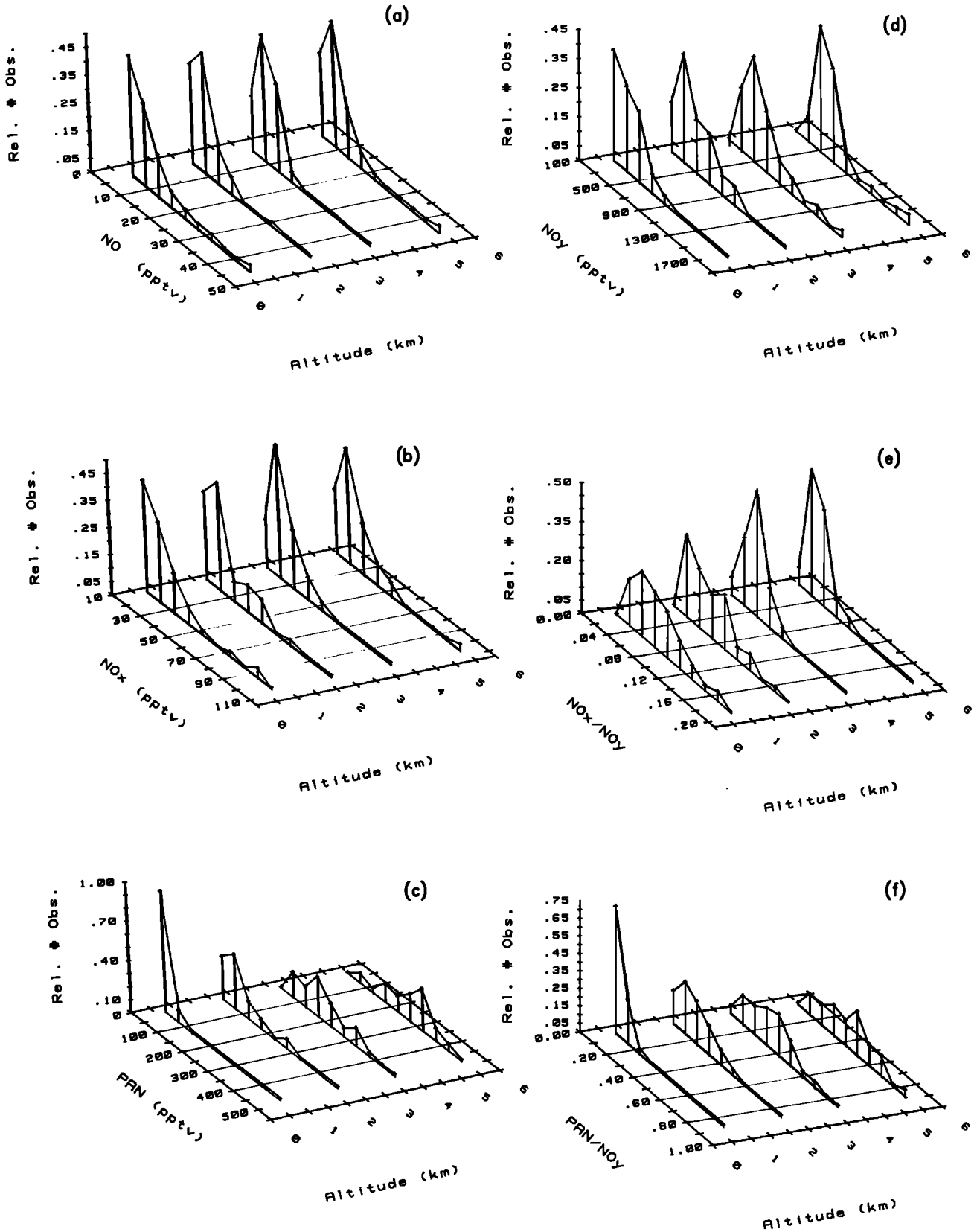

Fig. 6. Composites of vertical profiles taken over Alaska, where (*a*) NO, (*b*) NO_x, (*c*) PAN, (*d*) NO_y, (*e*) NO_x/NO_y, and (*f*) PAN/NO_y have been plotted in altitude ranges 0.1–1.5, 1.5–3.0, 3.0–4.5, and 4.5–6.1 km. The relative probability of occurrence for a species mixing ratio within each altitude range is presented on the *z* axis.

ratios of NO, NO_x, PAN, NO_y, and the individual fractions of NO_x/NO_y and PAN/NO_y. Statistical information for the mixing ratio distributions of each altitude range are given in Table 1. Mixing ratios of HNO_3 were not analyzed by our approach due to the long (30–90 min) sampling times used by this instrument. The general altitude trend for HNO_3 mixing ratios is discussed in the companion paper of *Singh et al.* [this issue (*b*)].

Mixing ratios of NO (Figure 6*a*) were filtered to include only those measurements made when the solar zenith angle was <67.5°. This limited the range of NO_2 photolysis rates (JNO_2), due solely to solar zenith angle, to about a factor of 2 for the 38° to 67.5° range of solar zenith angles occurring in this filtered data set. A composite of the JNO_2 values calculated for this filtered data set is given in Figure 10*f*. These JNO_2 values were calculated using an equation of the form given by *Chameides et al.* [1990] to extrapolate zenith and nadir viewing Eppley UV-photometer measurements. The larger than twofold range of JNO_2 values resulted from clouds lying above, below, or to the side of the aircraft, where either enhanced (for clouds below and to the side) or depressed (for clouds above) values of JNO_2 were encountered relative to clear-sky conditions. In some instances the increased albedo from the pack ice also enhanced JNO_2. Further filtering of NO mixing ratios based upon JNO_2 values was not done, as the remaining natural variance in JNO_2 is believed to represent a composite of typical daytime conditions occurring within about ±5 hours of solar noon.

NO mixing ratios measured at or below the instrumental limit of detection (LOD) represented <10% of this data set. Composites made from data sets in which these LOD data were omitted, or divided by factors of 1.5 or 2 yielded nearly identical distributions, means, and medians. Mean and median values differed by much less than the standard deviations between the different treatments of LOD data.

Mean and median NO mixing ratio values (~8.5 ± 2 pptv) were nearly identical and were close to the most probable mixing ratios measured in each altitude range except for possibly the lowest altitude range (0.15–1.5 km). At altitudes >1.5 km the vertical gradient in NO mixing ratios with altitude, implied from this composite, was small (<0.5 pptv/km).

The composite of NO_x ($NO + NO_2$) mixing ratios (Figure 6*b*), which was not solar zenith angle filtered, had a similar trend to that found for NO. Various treatments of the small fraction (<20%) of NO_x mixing ratios measured at or below the instruments LOD also had little effect on the tabulated values or mixing ratio distributions. Mean and median NO_x mixing ratios were also close in value (~25 ± 2 pptv) and exhibited little altitude dependency (<0.5 pptv/km). The slight tails and secondary maxima occurring in the distributions were also indicated in the distributions of several other compounds (e.g., CO and C_2H_2) and will be discussed in more detail later.

Unlike the mixing ratios of NO or NO_x, those of PAN and NO_y increased significantly in proportion to altitude (cf. Figures 6*a* and 6*b* versus 6*c* and 6*d*). Even though the distributions of both PAN and NO_y mixing ratios were somewhat broad and exhibited some indication of tails within the distributions, especially for the middle two altitude ranges (1.5–4.5 km), the mean and median values for each altitude range were reasonably close. Median PAN mixing ratios were found to increase by about 64 pptv/km, ranging from about 17 pptv in the lowest altitude range (0.15–1.5 km) to about 300 pptv at the highest (4.5–6.1 km). The altitude dependency of PAN mixing ratios accounted for all of the altitude gradient implied from the median mixing ratios of NO_y (~62 ppbv/km).

Average mixing ratios of PAN were correlated with those of NO_y (Figure 7*a*). However, average mixing ratios of NO_x were only slightly correlated with those of NO_y and were not significantly correlated with those of PAN (Figures 7*b* and 7*c*). Control of the abundance of NO_x and its relative uniformity within the lower 6-km column over Alaska has been attributed almost entirely to the thermal equilibrium of NO_x with PAN and other NO_x-containing compounds [*Singh et al.*, this issue (*b*); *Jacob et al.*, this issue]. Average mixing ratios of NO_x were also slightly correlated with those of CO, for CO mixing ratios ≤110 ppbv (Figure 7*d*). The possible significance of this correlation with measured trends in O_3 mixing ratios is discussed later.

Composites from individual ratios for NO_x/NO_y and PAN/NO_y measurements are illustrated in Figures 6*e* and 6*f*. Median ratios of NO_x/NO_y decreased nearly linearly with increasing altitude, as might be expected for the distribution shown for NO_x and NO_y, where median NO_x mixing ratios varied little with altitude, and NO_y mixing ratios increased in proportion to altitude. Median NO_x/NO_y fractions ranged from about 0.07 in the lowest altitude range to about 0.04 in the highest, a change of about 0.006/km. Median PAN/NO_y fractions exhibited the opposite trend; median values increased from about 0.05 in the lowest altitude range to about 0.47 in the highest, an increase of about 0.095/km that resulted in PAN accounting for about one-half of the NO_y abundance within the highest altitude range. Although not included in this analysis, HNO_3 mixing ratios measured on constant altitude flight legs did constitute the largest measured fraction of NO_y ($HNO_3/NO_y \sim 0.2$) within the lowest altitude range. Median HNO_3 mixing ratio values were about 65 pptv within the 0.15- to 1.5-km altitude range and like its precursor, NO_x, varied little with increasing altitude [*Singh et al.*, this issue (*b*)] (also S. Sandholm et al., Summertime partitioning and budget of NO_y compounds in the troposphere over Alaska and Canada: Arctic Boundary Layer Expedition (ABLE 3), submitted to *Journal of Geophysical Research*, 1992). Approximately 60 (±15)% of the NO_y abundance measured within the lowest altitude range could not be accounted for by NO_x, HNO_3, and PAN. This missing fraction of NO_y remained reasonably constant with altitude and was found to be in good agreement with measurements made at a ground site near Bethel, Alaska [*Bakwin et al.*, this issue]. Other more thermally stable NO_x-containing compounds have been suggested to represent about one-half of the NO_y measured within the lowest altitude range [*Bakwin et al.*, this issue; *Jacob et al.*, this issue].

Like NO_y and PAN, a strong altitude dependence was also observed for O_3 mixing ratios. Median mixing ratios of O_3 varied linearly from about 37 ppbv in the lowest altitude range to about 77 ppbv in the highest (cf. Figure 8*a*). The vertical gradient implied from the median mixing ratios (~9 ppbv/km) was slightly larger than that indicated by *Browell et al.* [this issue] for background air (5.5–7.5 ppbv/km). The difference between median O_3 mixing ratios in the highest two altitude ranges was, however, similar to that defined by Browell et al. for background air.

TABLE 1. Summary of Parameters

	NO	NO_x	PAN	NO_y	$\frac{NO_x}{NO_y}$	$\frac{PAN}{NO_y}$	O_3	CO	C_2H_2	C_2H_6	C_3H_8
										Altitude Range	
Mean	9.0	30	20	370	0.080	0.070	38	100	60	808	85
Median	7.2	22	17	350	0.066	0.051	37	95	56	818	86
s.d.	7.0	15	15	170	0.050	0.050	9	17	25	108	22
Min.	2.2	9.8	7	150	0.021	0.011	22	82	28	627	48
Max.	43	96	86	810	0.29	0.21	63	149	210	1060	164
n	74	60	48	79	60	40	96	86	65	65	65
										Altitude Range	
Mean	8.5	30	85	480	0.065	0.20	54	103	70	851	89
Median	8	22	67	420	0.059	0.19	53	98	53	833	84
s.d.	4.5	15	60	230	0.035	0.10	12	17	30	147	30
Min.	2.6	10	19	170	0.02	0.026	30	85	0	631	40
Max.	29	74	270	1100	021	0.55	98	152	161	1349	226
n	81	70	46	84	70	37	106	96	73	74	74
										Altitude Range	
Mean	9.5	27.5	190	640	0.050	0.30	70	107	80	878	88
Median	9.2	27	180	570	0.047	0.36	70	100	65	853	80
s.d.	3.5	9.5	85	290	0.020	0.15	13	21	45	131	27
Min.	3.7	13	60	260	0.013	0.05	37	87	40	671	49
Max.	17	52	380	1700	0.099	0.71	102	180	270	1296	172
n	86	73	54	91	73	43	117	107	80	80	80
										Altitude Range	
Mean	9.5	30	280	700	0.040	0.45	77	106	85	927	116
Median	8.3	25	300	610	0.039	0.47	77	102	79	111	103
s.d.	6.0	15	110	310	0.015	0.20	13	14	25	932	38
Min.	2.6	12	85	360	0.011	0.11	40	85	40	678	67
Max.	47	110	700	1800	0.083	0.90	108	142	150	1314	208
n	80	63	45	82	63	37	107	96	59	59	59

NO, NO_x, PAN, NO_y, C_2H_2, C_2H_6, C_3H_8, and C_2Cl_4 are all in units of pptv; O_3 and CO are in units of ppbv; temperature (Temp.) is in degrees Celsius; is in H_2O is in parts per thousand (pptv); and the ratios NO_x/NO_y and PAN/NO_y are pptv/pptv, where the means or medians are of the ratios (not ratios of means or medians). Potential temperature is in degrees Kelvin; the ratios of NO_y/O_3 and C_3H_8/C_2H_6 are in units of pptv/pptv; the ratio C_2H_2/CO is in pptv/ppbv; JNO_2 is in units of s^{-1}; and the other ratios are unitless; means or medians are of the ratios (not ratios of the means or medians).

Median values of the individual ratios of NO_y/O_3 were nearly independent of altitude and were close to the most probable values for each altitude range (i.e., median NO_y/O_3 ~0.0075; cf. Figure 8*b*). These trends in the NO_y/O_3 ratio were very similar to the general trends and range of values summarized by *Murphy et al.* [1992] for several other remote tropospheric locations not overly perturbed by lightning activity (NO_y/O_3 ~ 0.005–0.01).

Correlative tendencies between average mixing ratios of O_3 and those of NO_x, PAN, NO_y, and CO are depicted in Figure 9. The degree of correlation between average mixing ratios of O_3 versus those of PAN and NO_y was expected based upon the altitudinal dependencies revealed. The slope of the regression between mixing ratios of O_3 and NO_y (slope ~0.07 ppbv/pptv) falls within the range of values summarized by *Hübler et al.* [1992] (slope ~0.06–0.11) for lower latitude free tropospheric measurements. This general correlation between O_3 and NO_y appears to be a relatively consistent feature within the northern hemisphere's free troposphere.

The tendency toward correlation between mixing ratios of O_3 and NO_x, at small NO_x mixing ratios (i.e., $NO_x \leq 40$ pptv) was not anticipated from the trends in O_3 and NO_x mixing ratios with altitude. This on-average correlation could suggest a nearly linear 1 ppbv ΔO_3/1 pptv ΔNO_x relationship for NO_x mixing ratios <40 pptv. A similar tendency toward correlation occurred between mixing ratios of O_3 and CO, for CO mixing ratios ≤110 ppbv. The nearly 1 ppbv ΔO_3/1 ppbv ΔCO relationship implied from the regression (for CO ≤ 110 ppbv) also suggests air mass aging processes may have been important factors controlling the abundance of these compounds. The apparent falloff of the on-average relationship at NO_x mixing ratios larger than about 40 pptv could result from an insufficient time for NO_x to have photochemically impacted O_3 abundance. Indeed, the >40 pptv tails of the NO_x distribution may represent less aged air with relatively fresh NO_x inputs from short-range sources such as high-latitude biomass burning. This correlation between O_3 and NO_x (at $NO_x \leq 40$ pptv) tends to support the model analyses of *Jacob et al.* [this issue]. These analyses suggested an approximate doubling in the midtropospheric lifetime of O_3 for the median NO mixing ratio measured during ABLE 3A versus the O_3 lifetime calculated in absence of NO.

4.2.2. *Estimate of photochemical O_3 production versus destruction.* A simplified analysis based on in situ measurements can be used for an assessment of the balance between photochemical O_3 production versus destruction for air masses described by this composite data set. Following the general treatment recently summarized by *Ridley* [1991], photochemical O_3 production is controlled by the reactions:

(R1) $HO_2 + NO \rightarrow NO_2 + OH$, k_1

for the Vertical Composite

C_2Cl_4	Temp.	H_2O	Pot. Temp.	$\frac{NO_y}{O_3}$	$\frac{C_2H_2}{CO}$	$\frac{C_3H_8}{C_2H_6}$	JNO_2	$\frac{NO_{eq(1)}}{NO}$	$\frac{NO_{eq(2)}}{NO}$	$\frac{NO_2(c)}{NO_2(m)}$	$\frac{O_{3eq}}{O_3}$
0–1.5 km											
10.5	8.5	8.5	289	0.0105	0.57	0.105	0.0078	0.90	2.0	1.07	1.00
11	8.8	8.7	290	0.0082	0.58	0.1	0.0074	0.82	1.8	0.92	0.11
1.0	4.0	2.0	5	0.0055	0.12	0.020	0.0029	0.50	1.5	0.82	3.0
8	−3.1	2.5	271	0.0036	0.33	0.055	0.0024	0.13	0.24	0.059	−0.74
13	19	13	297	0.025	0.85	0.16	0.0169	2.5	6.9	3.85	16
37	96	96	96	79	58	65	87	74	72	55	55
1.5–3 km											
11.0	1.0	5.0	296	0.0095	0.61	0.105	0.0099	1.05	2.0	0.97	0.50
12	1.5	5.0	296	0.0072	0.55	0.11	0.0089	0.94	2.5	0.81	0.33
1.5	3.5	2.5	4	0.0050	0.18	0.020	0.0032	0.45	1.5	0.63	1.0
8	−7.7	0.84	284	0.0030	0.40	0.046	0.0033	0.34	0.86	0.17	−0.67
14	8.1	9.6	304	0.028	1.1	0.17	0.0171	2.5	7.1	3.04	5.0
45	106	106	106	84	66	74	97	81	78	65	65
3–4.5 km											
12.5	−7.0	2.5	304	0.0090	0.73	0.10	0.1083	1.05	2.25	0.82	0.70
12	−6.5	2.4	304	0.0076	0.69	0.099	0.0103	0.98	2.1	0.76	0.33
1.0	4.0	1.5	4	0.0050	0.24	0.020	0.0026	0.40	0.95	0.46	1.0
8	−17	0.35	295	0.0040	0.43	0.055	0.0065	0.56	0.88	0.19	−0.59
17	0.53	6.5	312	0.028	1.6	0.16	0.0165	3.0	5.7	2.46	4.2
52	120	120	117	91	74	80	109	86	84	67	67
4.5–6.1 km											
13.5	−16.0	1.20	311	0.0092	0.75	0.120	0.01178	1.20	2.5	0.58	2.0
13	−16	0.90	311	0.0080	0.16	0.12	0.01135	1.1	2.1	0.48	1.1
2.0	4.0	0.80	4	0.0045	0.73	0.030	0.00251	0.60	1.5	0.40	2.0
10	−29	0.28	301	0.0051	0.45	0.075	0.00739	0.18	0.65	0.11	−0.48
18	−7.0	3.6	321	0.029	1.1	0.19	0.01651	3.6	8.4	1.92	8.0
45	110	110	109	80	53	59	99	78	73	54	54

(R2) $RO_2 + NO \rightarrow NO_2 + RO,\ k_2$

where each NO_2 molecule formed via (R1) and (R2) is assumed, upon photolysis, to yield an O_3 molecule. The photochemical O_3 production rate, $PR(O_3)$, is directly dependent on the concentration of NO and can be expressed by the equation

$$PR(O_3) = (k_1[HO_2] + k_2[RO_2])[NO] \quad (1)$$

The loss processes of O_3, under conditions typical of these air masses, is primarily controlled by the reactions

(R3) $O_3 + h\nu \rightarrow O(^1D) + O_2,\ JO_3,$

followed by

(R4) $O(^1D) + H_2O \rightarrow 2OH,\ k_4,$

versus

(R5) $O(^1D) + M \rightarrow O(^3P) + M,\ k_q;$

(R6) $HO_2 + O_3 \rightarrow HO + 2O_2,\ k_6;$

and

(R7) $O_3 \rightarrow$ surface removal, k_d.

The loss rate of O_3, $LR(O_3)$, based upon reactions (R3)–(R7), is given by

$$LR(O_3) = (k_6[HO_2] + BR\ JO_3 + k_d)[O_3], \quad (2)$$

where the $O(^1D)$ branching ratio BR is given by

$$BR = k_4[H_2O]/(k_q[M] + k_4[H_2O]). \quad (3)$$

From (1) and (2) the equivalent concentration of NO, $[NO_{eq}]$, needed for a zero net rate of O_3 production (i.e., $PR(O_3) = LR(O_3)$) can be estimated by

$$[NO_{eq}] = \frac{(k_6[HO_2] + BR\ JO_3 + k_d)[O_3]}{(k_1[HO_2] + k_2[RO_2])}. \quad (4)$$

Equation (4) can be further simplified to the form

$$[NO_{eq1}] = \frac{k_6[HO_2][O_3]}{k_1[HO_2] + k_2[RO_2]} \approx \frac{k_6[O_3]}{1.4k_{1-2}}, \quad (5)$$

for remote free tropospheric conditions, where CH_3O_2 represents the dominant RO_2 compounds with $[RO_2] \sim 0.4[HO_2]$ [e.g., *Logan et al.*, 1981], and for $k_1 \sim k_2 \sim k_{1-2} \sim 4 \times 10^{-12}$ exp (210/T) with k_{1-2} representing the average of k_1 and k_2 (rate coefficients from *DeMore et al.* [1990]). Equation (5) represents the smallest abundance of NO necessary for net photochemical production and provides a useful reference point for comparisons involving the additional assumptions necessary to evaluate (4).

For the NO_x mixing ratios measured over Alaska (i.e., $NO_x < 100$ pptv), the concentration of peroxy radicals has been predicted to be nearly independent of NO_x concentra-

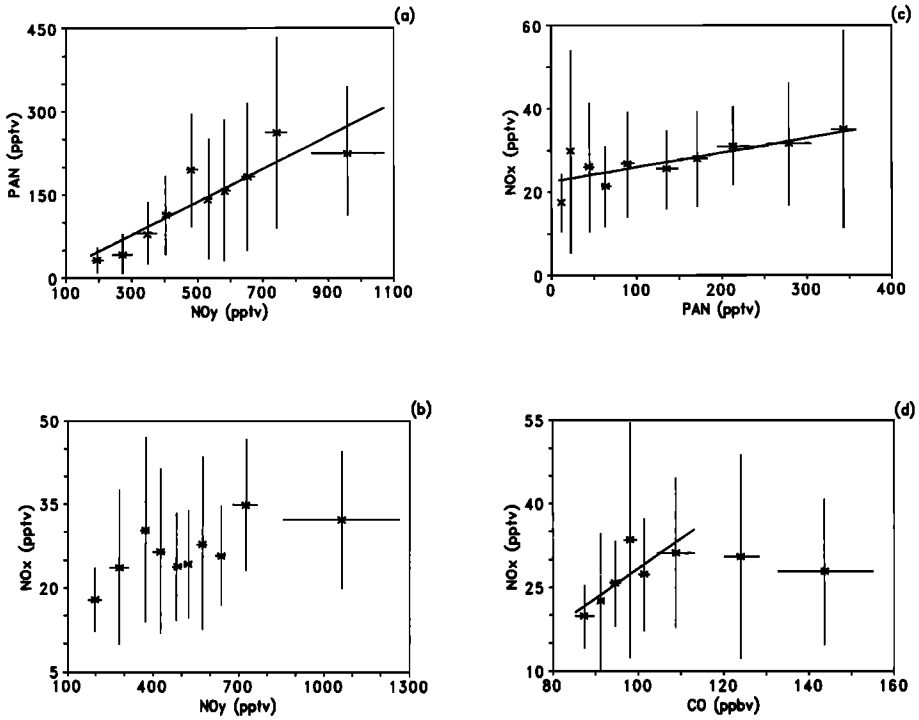

Fig. 7. Correlation plots of aggregated data, where the horizontal and vertical lines represent ±1 sigma about the mean of the aggregate: (*a*) PAN versus NO_y with an aggregate size (AS) of 15 measurements (r^2 = 0.80 and slope of 0.30 ± 0.05), (*b*) NO_x versus NO_y with AS = 26 (r^2 = 0.52 and slope of 0.014 ± 0.0049), (*c*) NO_x versus PAN with AS = 15 (r^2 = 0.59 and slope of 0.034 ± 0.010), (*d*) NO_x versus CO with AS = 31 (for the first six aggregates, r^2 = 0.63, and slope of 0.53 ± 0.20).

tion [e.g., *Logan et al.*, 1981]. These estimates also indicated mixing ratios of peroxy radicals were relatively independent of altitude within the lower 6-km column near 60°N, with ($[HO_2]$ + $[RO_2]$)/[M] ~ 25 pptv. A simplification of (4), which neglects k_d, but includes an estimation of the direct photolytic loss of O_3, is given by

$$[NO_{eq2}] = \frac{k_1[O_3]}{1.4k_{1-2}} + \frac{BR\ JO_3[O_3]}{k_{1-2}([HO_2] + [RO_2])}. \quad (6)$$

Equations (5) and (6) were evaluated using the assumptions described above and for the individual O_3, H_2O, and temperature measurements within the composite data set. The O_3 photolysis rate, JO_3, was derived from the estimates of *Demerjian et al.* [1980] using a parameterized fit, which was similar to that described for JNO_2 by *Parrish et al.* [1981], given by

$$JO_3 = a(\exp [b \sec \chi]), \quad (7)$$

where a and b are linearly fit functions of albedo (α) and altitude (2) (e.g., $a = c + d\alpha + e2$) and χ is the solar zenith angle. These clear-sky JO_3 values were normalized to JNO_2 values calculated from the Eppley UV-photometers using similarly parameterized clear-sky estimates of JNO_2. This normalization produced results equivalent to those described by *Chameides et al.* [1990] for the normalization of clear-sky two-stream model photolysis rate estimates. This normalization, based on nadir and zenith Eppley UV-photometers, was assumed to provide a first-order correction for varying albedo. This correction was also assumed to be wavelength independent over the range of 300–400 nm. In addition, JO_3 values were also corrected for daily total O_3 column over the study region using the tabulated total ozone mapping spectrometer (TOMS) 1988 data. For clear-sky conditions, comparison of values obtained from these parameterized photolysis rate equations to those derived from a two-stream model have agreed to better than ±20% over the range of solar zenith angles contained within this filtered data set ($38° < x < 67.5°$).

Figures 10*a* and 10*b* depict the ratios NO_{eq1}/NO_{meas} and NO_{eq2}/NO_{meas}, where NO_{meas} was the measured mixing ratio coincident with measurements of O_3, H_2O, temperature, pressure, and UV solar flux. A nearly constant value of $[NO_{eq1}]$ with altitude could be predicted from (5), based on the small temperature dependencies of the rate coefficients [*DeMore et al.*, 1990] and the nearly constant median concentration of O_3 versus altitude (~1 × 10^{12} O_3/cm^3; cf. Figure 8*a*). Median NO_{eq1}/NO_{meas} ratios were near unity and varied only slightly with altitude, indicating measured NO mixing ratios were close to the lower limit for net O_3 production estimated from (5). Median NO_{eq2}/NO_{meas} ratios were about twofold larger and also varied only slightly with altitude. The small altitude dependency implied for NO_{eq2} was due, in part, to the nearly constant terms (k and $[O_3]$) discussed for (5) and the nearly constant value for $BR\ JO_3/[HO_2]$. The nearly fourfold smaller value of BR occurring in the highest versus the lowest altitude range was almost completely offset by the nearly twofold smaller values of $[HO_2]$ + $[RO_2]$ (for constant mixing ratios of HO_2 + RO_2), and the nearly twofold larger values of JO_3. These results suggest that the photochemical O_3 loss rate via

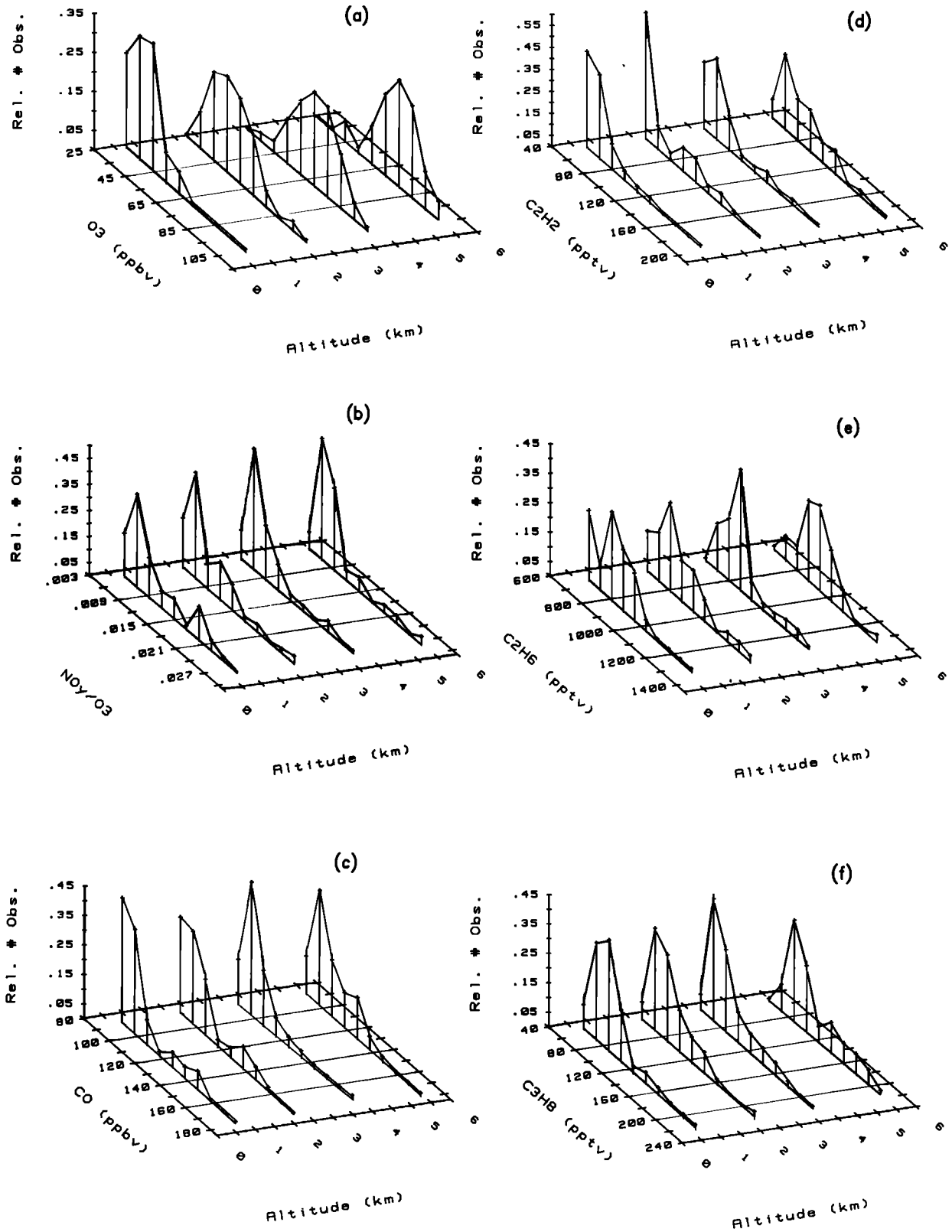

Fig. 8. Composites of vertical profiles taken over Alaska, where (*a*) O_3, (*b*) NO_y/O_3, (*c*) CO, (*d*) C_2H_2, (*e*) C_2H_6, and (*f*) C_3H_8 have been plotted in altitude ranges 0.1–1.5, 1.5–3.0, 3.0–4.5, and 4.5–6.1 km. The relative probability represented on the *z* axis is described in Figure 6.

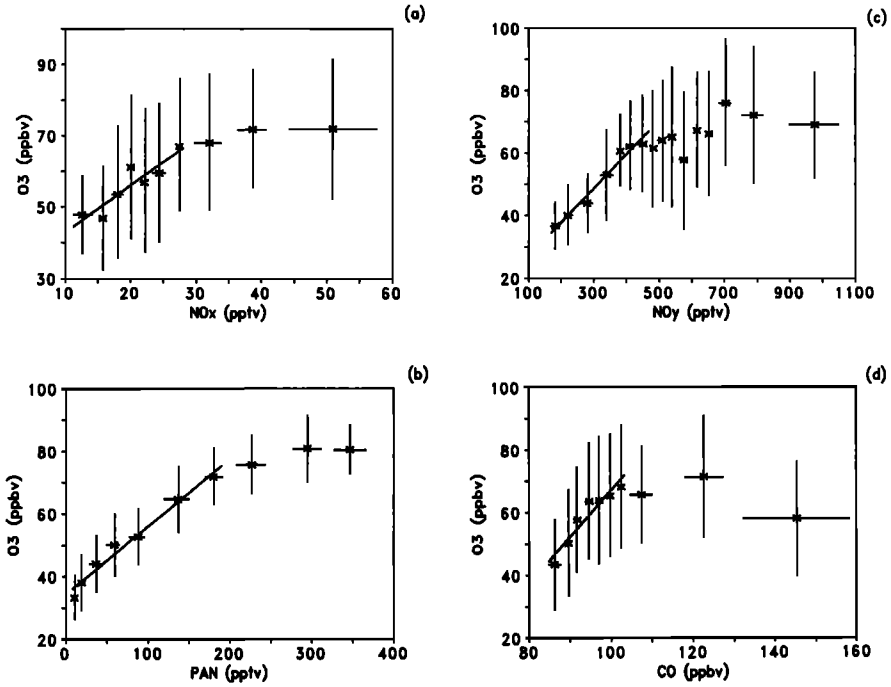

Fig. 9. Correlation plots for aggregated data, where the horizontal and vertical lines represent ±1 sigma about the mean of the aggregate: (*a*) O_3 versus NO_x with an aggregate size (AS) of 26 measurements ($r^2 = 0.79$ for all aggregates and $r^2 = 0.84$ for the first seven aggregates with a slope of 1.32 ± 0.26), (*b*) O_3 versus PAN with AS = 19 ($r^2 = 0.92$ for all aggregates and $r^2 = 0.98$ for the first seven aggregates with a slope of 0.22 ± 0.015), (*c*) O_3 versus NO_y with AS = 20 ($r^2 = 0.71$ for all aggregates and $r^2 = 0.97$ for the first seven aggregates with a slope of 0.109 ± 0.0091), (*d*) O_3 versus CO with AS = 38 ($r^2 = 0.74$ for all aggregates and $r^2 = 0.90$ for the first seven aggregates with a slope of 1.48 ± 0.22).

(R3)–(R5) was of comparable magnitude to that occurring via (R6). In addition, these estimates suggest that, on average, mixing ratios of NO were about twofold smaller than those required to balance the photochemical rates of O_3 loss and production.

In the companion paper of *Jacob et al.* [this issue], clear-sky photochemical model calculations predicted significant net O_3-photochemical loss throughout most of the lower 6-km column over Alaska (-1.8×10^5 molecules cm^{-3} s^{-1} diurnally averaged). The estimates presented here are in generally good agreement with the model calculations of Jacob et al., although some differences occur at the lowest and highest altitudes. These differences were likely due to differences in the data set analyzed (e.g., the data set analyzed by Jacob et al. included a large fraction of data taken within the mixed layer over the tundra). Even so, their estimates within the 1.5- to 5-km altitude range also indicated that the median NO mixing ratios measured over Alaska were approximately twofold smaller than those required to balance O_3 photochemical production and loss.

These NO_{eq}/NO_{meas} estimates are, however, in apparent disagreement with the one-dimensional model results presented in the companion paper of *Singh et al.* [this issue (*b*)]. This latter evaluation compared calculated mixing ratios of NO_x necessary for net photochemical production to the median values of NO_x measured over Alaska. Comparison of their NO_x-based analysis to the NO-based analyses discussed above requires an examination of the photostationary state relationship between NO_2 and NO.

4.2.3. *NO_2/NO photostationary state implication on peroxy radical concentrations.* The daytime steady state ratio of $[NO_2]/[NO]$ is controlled primarily by the reactions (R1), (R2); (R8), (R9), involving

(R8) $$NO + O_3 \rightarrow NO_2 + O_2, k_8;$$

(R9) $$NO_2 + h\nu \rightarrow NO + O, J_{NO_2}.$$

The steady state ratio of $[NO_2]/[NO]$ is given by

$$[NO_2]/[NO] = (k_8[O_3] + k_1[HO_2] + k_2[RO_2])/J_{NO_2} \quad (8)$$

Under atmospheric conditions where $[HO_2]$ and $[RO_2]$ are suppressed (e.g., $[NO_x] > 1$ ppbv), (8) can be reduced to the simple photostationary state relationship:

$$[NO_2]/[NO] = k_8[O_3]/J_{NO_2}. \quad (9)$$

From (9) an estimate of the smallest abundances of NO_2 (NO_{2calc}) can be obtained from measurements of NO, O_3, temperature, pressure, and UV solar flux. Figure 10*c* depicts the solar zenith angle filtered ($38° < \chi < 67.5°$) composite for the ratio NO_{2calc}/NO_{2meas} using (9) and measured mixing ratios of NO_2. Median values of this ratio were less than unity, as expected for exclusion of reactions (R1) and (R2) in describing NO_{2calc}/NO_{2meas} for these relatively clean air masses.

The measured ratio $[NO_2]/[NO]$ can be expressed by an equation of the form

$$\{[NO_2]/[NO]\}_{meas} = k_8([O_3]_{meas} + [O_3]_{eq})/J_{NO_2}, \quad (10)$$

where $[O_3]_{eq}$ represents the concentration of the often termed "missing-oxidant" in units equivalent to those of O_3. For HO_2 and RO_2 representing the missing oxidants, O_{3eq} can be expressed by

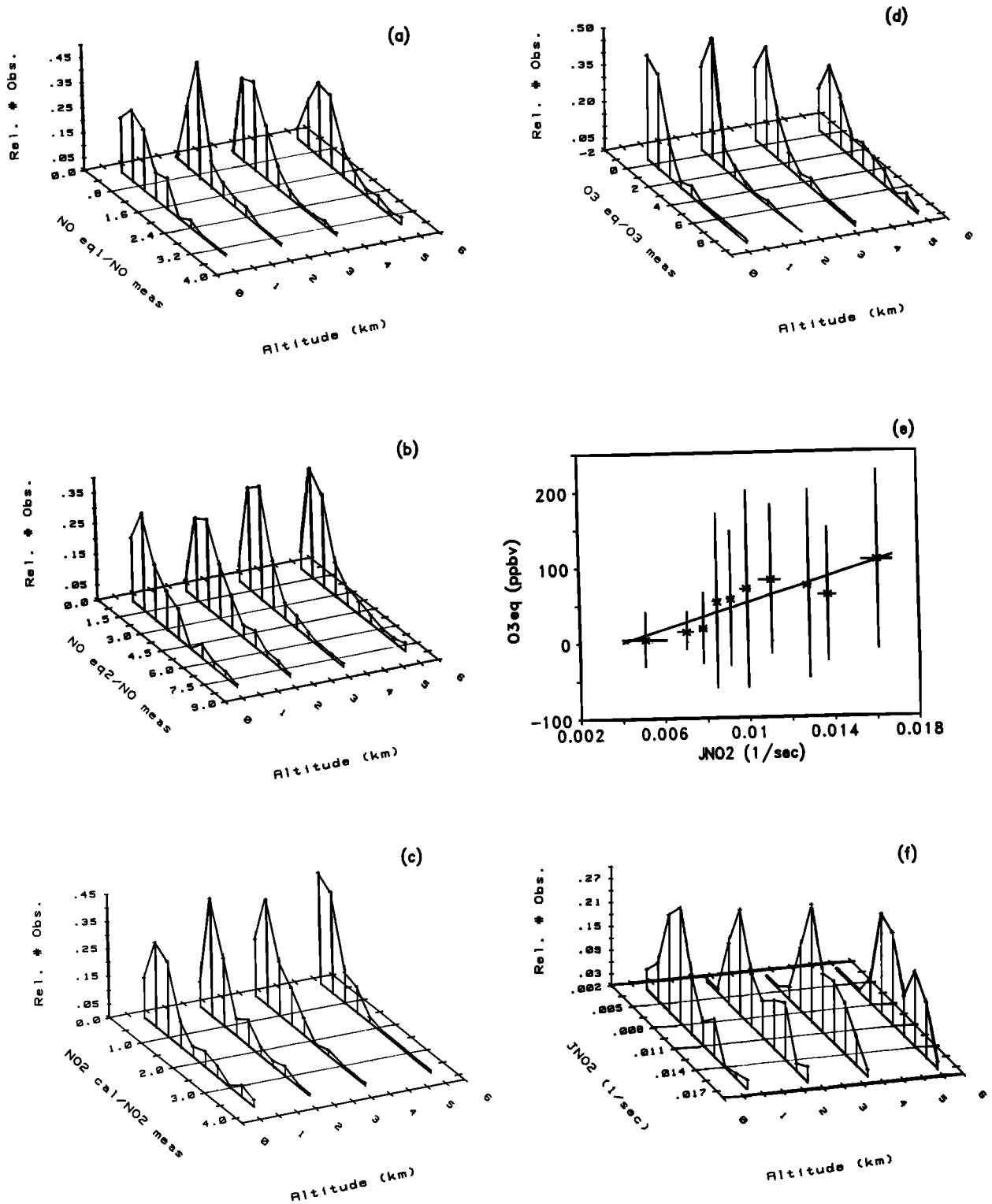

Fig. 10. Composite vertical sounding over Alaska, where (*a*) NO_{eq1}/NO_{meas}, (*b*) NO_{eq2}/NO_{meas}, (*c*) NO_{2calc}/NO_{2meas}, (*d*) O_{3eq}/O_{3meas}, and (*f*) JNO_2 have been plotted in altitude ranges 0.1–1.5, 1.5–3.0, 3.0–4.5, and 4.5–6.1 km. The relative probability within an altitude range is represented on the *z* axis. (*e*) A correlation plot of aggregated data, where the horizontal and vertical lines represent ±1 sigma about the mean of the aggregate for O_{3eq} versus JNO_2 with an aggregate size of 24 measurements ($r^2 = 0.79$ and slope of 8700 ± 1600).

$$[O_3]_{eq} = (k_1[HO_2] + k_2[RO_2])/k_8. \quad (11)$$

Figure 10*d* depicts the ratio of $[O_3]_{eq}/[O_3]_{meas}$ calculated from (10). Within the middle two altitude ranges (1.5–4.5 km), median values of this ratio suggest the equivalent O_3 mixing ratios needed to balance (10) were about one-third as large as those measured. Based on (11) and for $k_1 \sim k_2$, these O_{3eq} mixing ratios correspond to mixing ratios of $HO_2 + RO_2$ of about 20 pptv. This value is in the range of those taken from *Logan et al.* [1981] and used earlier in the

assessment of NO_{eq2}. Median values calculated for the ratio O_{3eq}/O_{3meas} within the lowest altitude range suggest a small contribution from peroxy radicals on the photostationary state of the mixed layer. This estimate is in general agreement with the analyses by *Bakwin et al.* [this issue] for surface measurements of NO_2 and NO near Bethel.

Larger median mixing ratios of $HO_2 + RO_2$ (~75 pptv) were, however, implied from our calculations for the highest altitude range. This latter results, in conjunction with the large difference between mean and median O_{3eq}/O_{3meas} ratios, suggests a more complete understanding of the NO_2/NO photostationary state relationships preliminarily investigated here may require (1) refined model calculations, which incorporate actual conditions (e.g., the use of actual hydrocarbon abundances, representation of actual cloud fields, and changes in total O_3 column), and (2) reinvestigation of small possible interferences in measured NO_2 (e.g., 5–10 pptv of thermally/photolytically derived interference from 100-fold larger mixing ratios of unaccounted for NO_y compounds). These results also suggest that without such reanalyses, which are in progress, comparisons of the model-calculated mixing ratios of NO_x necessary for photochemical O_3 production to mixing ratios of NO_x that were measured may be less interpretable than similar analyses based on NO mixing ratios.

The mixing ratios of NO were more directly measured than those of NO_2, allowing higher immunity to interferences, and absolute accuracy. Based on the preceding discussions, we believe the NO-based analyses more accurately describe the role of NO on the photochemical lifetime of O_3. We find that on average the NO mixing ratios measured over Alaska were about twofold smaller (within the 1.5- to 5-km altitude range) than those necessary to balance the photochemical rates of O_3 production and loss.

4.2.4. *Distributions and trends of representative carbon-containing compounds.* The compounds CO and C_2H_2, which are primarily products of combustion, also exhibited altitude dependencies in their median mixing ratios (~1 ppbv/km for CO and ~5 pptv/km for C_2H_2; cf. Figures 8*c* and 8*d*). However, the most probable portion of the mixing ratio distributions for these compounds varied only slightly with altitude. The pronounced tails and secondary maxima in their distributions contributed to most of the differences (~10–15% for CO and 20–30% for C_2H_2) between the most probable and the median mixing ratios for these compounds. Similar tendencies were also measured for mixing ratios of C_2H_6, and C_3H_8 (cf. Figures 8*e* and 8*f*), even though these latter compounds have both combustion- and noncombustion-related sources. These similarities may represent the effects of either common sources (or source regions) or sinks for these compounds.

The ratios formed from various carbon-containing compounds are useful as indicators of relative air mass age when the compounds chosen share common sources and sinks [e.g., *Singh and Zimmerman*, 1992]. The primary tropospheric sink for the carbon-containing compounds discussed here is their oxidation by OH radicals via either H atom abstraction (C_2H_6, C_3H_8) or O atom addition (CO, C_2H_2). H atom abstraction reactions are temperature dependent and would have had rate coefficients that varied by about ±35% over the temperature ranges encountered in ABLE 3A [*DeMore et al.*, 1990]. For a diurnally averaged OH concentration of about 1×10^6 OH/cm^3 [*Jacob et al.*, this issue], the tropospheric lifetime of C_2H_6 would have been of the order of 60 ± 20 days and that of C_3H_8 about 14 ± 4 days. The O atom addition reactions are far less temperature dependent, but as three-body reactions they do depend slightly (< ±20%) on pressure over the pressure range encountered during ABLE 3A (0.5–1 atm) [*DeMore et al.*, 1990]. The tropospheric lifetime of CO (~54 ± 12 days) would have been similar to that estimated for C_2H_6, and the lifetime of C_2H_2 (~14 ± 4 days) would have been similar to that estimated for C_3H_8. The overall uncertainty in these lifetime estimates would most likely be much larger than indicated by the pressure and temperature dependencies of the rate coefficients, due to uncertainties in the estimates of average OH concentrations and the exclusion of surface sink terms. Even so, these estimates could be useful in describing the general trends that might be expected between compounds and the order of magnitude of their lifetimes in relation to transport time (Δt) from distant sources. The relative difference in elapsed time (equated here to transport time Δt) for compounds with different chemical lifetimes can be approximated by

$$\Delta t = \frac{\ln [(C_A/C_B)_{t1}/(C_A/C_B)_{t2}]}{(k_A - k_B)C_{OH}} \quad (12)$$

where C_A, C_B are the concentration of compounds A and B at times $t1$ and $t2$, having reaction rate coefficients k_A and k_B, and C_{OH} is the OH concentration.

Mixing ratios of C_2H_2 were significantly correlated ($r^2 \sim 0.87$) with those of CO (slope ~1.7 pptv/ppbv; Figure 12*a*) as might be expected from compounds that share both common sources (i.e., combustion) and sinks (i.e., oxidation via O atom addition reactions involving OH). The composite of individual C_2H_2/CO ratios (Figure 11*a*) exhibited an increase in median values in proportion with altitude. This trend could suggest an influx of less aged (Δt ~20–30%) air into the 4- to 6-km altitude range.

Average mixing ratios of C_2H_6 and C_3H_8 were also correlated with those of CO (cf. Figures 12*b* and 12*c*). In addition, the average ratio of C_3H_8/C_2H_6 was correlated with ratios of C_2H_2/CO, which suggests common factors (either sources or sinks) were controlling the mixing ratios of all of these compounds. The regression of ln (C_3H_8/C_2H_6) versus ln (C_2H_2/CO) yielded about a threefold smaller slope than expected from (12), based upon equivalent transport times (Δt), OH concentrations, and rate coefficients representative of the tropospheric conditions encountered (i.e., expected slope ~1.1 versus ~0.4; cf. Figure 12*d*). Although very qualitative, this could suggest various source emission factors (signatures) were a more important factor than the OH photochemical sink in controlling the average relationships observed for these compounds. Relative emission factors (e.g., $\Delta C_2H_2/\Delta CO$ and $\Delta C_3H_8/C_2H_6$) were found to vary significantly even for similar types of sources (e.g., high-latitude biomass burning $\Delta C_2H_2/\Delta CO \sim 0.002$–0.03 and $\Delta C_3H_8/\Delta C_2H_6 \sim 0.1$–0.3 [*Wofsy et al.*, this issue] (also D. R. Blake et al., Nonmethane hydrocarbons in the troposphere over central Canada, submitted to *Journal of Geophysical Research*, 1992) and similar variances for industrial/urban emissions [*Warnek*, 1988; *Singh and Zimmerman*, 1992]).

Even though significant uncertainties (factors of twofold to threefold) exist in estimated transport times based on hydrocarbon ratios, the small values of C_3H_8/C_2H_6 mea-

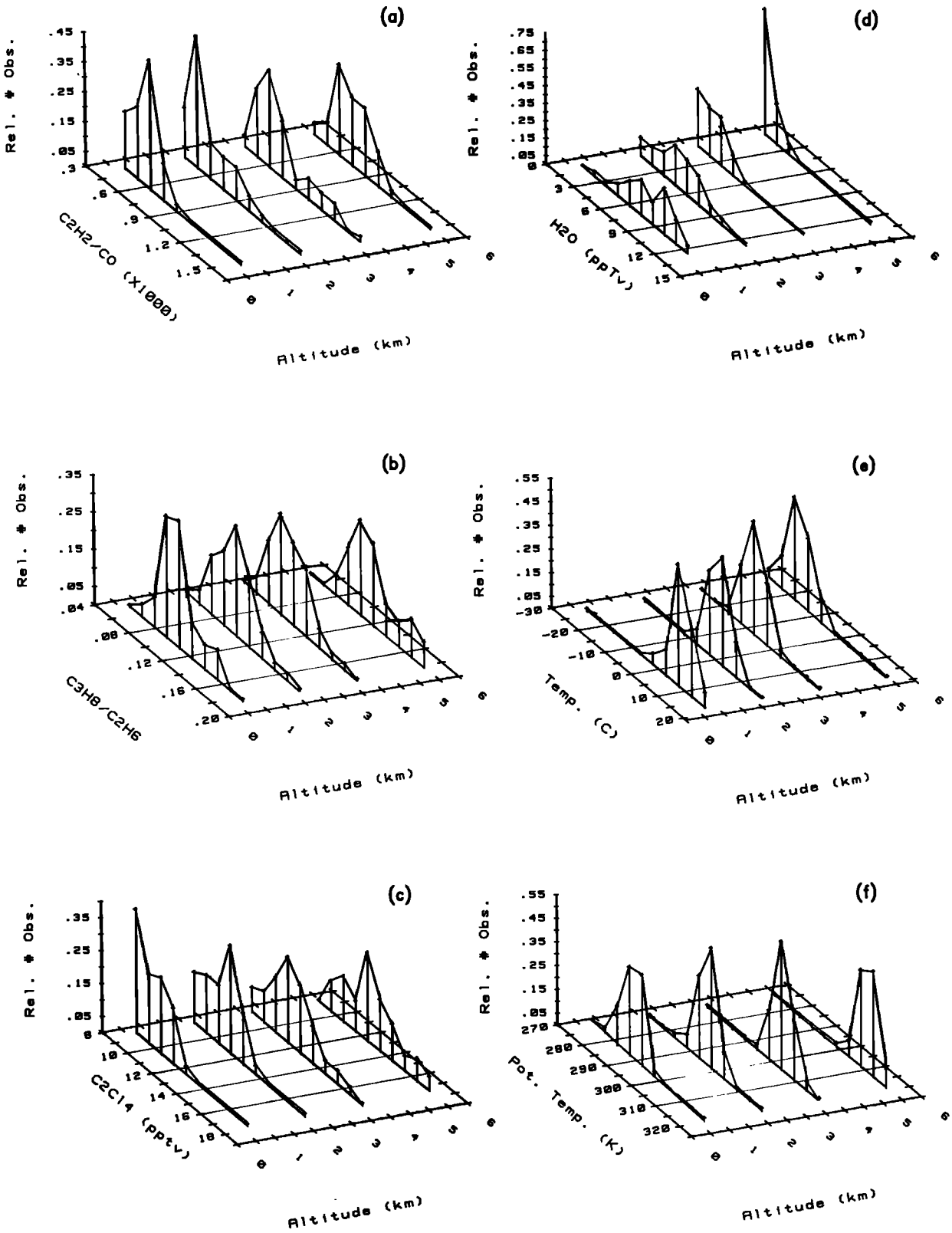

Fig. 11. Composites of vertical profiles taken over Alaska, where (*a*) C_2H_2/CO, (*b*) C_3H_8/C_2H_6, (*c*) C_2Cl_4, (*d*) H_2O, (*e*) static air temperature, and (*f*) potential temperature have been plotted in altitude ranges of 0.1–1.5, 1.5–3.0, 3.0–4.5, and 4.5–6.1 km. The relative probability represented on the *z* axis is as described in Figure 6.

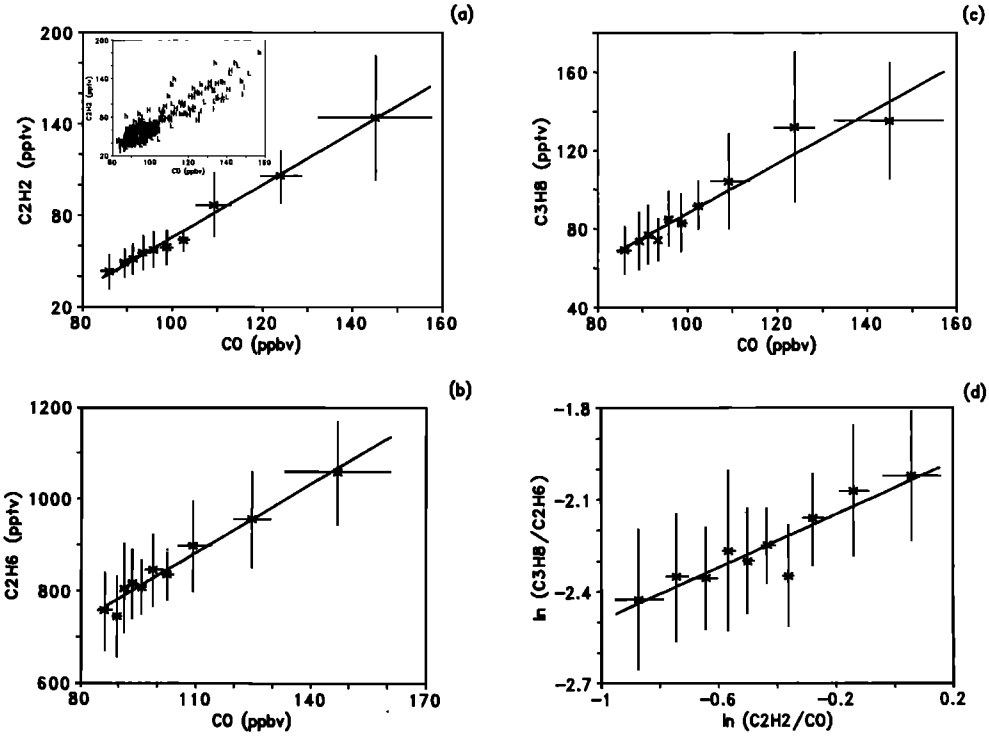

Fig. 12. Correlation plots of aggregated data, where the horizontal and vertical lines represent ±1 sigma about the mean of the aggregate. (*a*) C_2H_2 versus CO with an aggregate size (AS) of 25 measurements (r^2 = 0.99 and slope of 1.73 ± 0.065). The insert represents individual measurements with interior labels: l (0.1–1.5 km), L (1.5–3.0 km), h (3.0–4.5 km), and H (4.5–6.1 km). (*b*) C_2H_6 versus CO with As = 24 (r^2 = 0.97 and slope of 5.01 ± 0.33). (*c*) C_3H_8 versus CO with AS = 24 (r^2 = 0.93 and slope of 1.26 ± 0.12). (*d*) Plot of ln (C_3H_8/C_2H_6) versus ln (C_2H_2/CO) with AS = 25 (r^2 = 0.84 and slope of 0.43 ± 0.065).

sured over Alaska suggest mid-latitude industrial/urban emissions transported into this region would have been relatively well aged. Transport times of 15–30 days were estimated from the C_3H_8/C_2H_6 (~0.1) ratios measured over summertime Alaska versus ratios reported for industrial pollution (0.4–0.8 [e.g., *Warnek*, 1988; *Doskey and Gaffney*, 1992]), and assuming a constant OH concentration. These transport times were of the order of those predicted by the analyses of *Patterson and Husar* [1981] for the summertime transport of pollutants to Alaska from population centers in eastern North America, northern Europe, and the area near the Sea of Japan (on average $\Delta t \geq 20$ days).

Less distant sources could have also influenced the measured hydrocarbon ratios (e.g., biomass burning in Siberia and Alaska, $\Delta C_3H_8/\Delta C_2H_6 \sim 0.1$–0.3, and gas/oil production/leakage from regions such as Russia, $\Delta C_3H_8/\Delta C_2H_6 \sim 0.1$–0.7 [*Blake et al.*, this issue]). The influence of more regional-scale emissions with <5-day transport times would not be easily distinguished from the influence of more distant sources, especially in the case of regional biomass burning where the $\Delta C_3H_8/\Delta C_2H_6$ emission factors are expected to have small but variable values.

4.2.5. *Trends between carbon-containing compounds, N_xO_y, and O_3.* Unlike the carbon-containing compounds just discussed, the synthetic compound C_2Cl_4 exhibited an altitude dependency in its mixing ratio distributions similar to the dependencies found for PAN and O_3 (cf. Figure 11*c*). Median mixing ratios of C_2Cl_4 increased porportionally with altitude by about 0.8 pptv/km. The estimated lifetime for C_2Cl_4 oxidation by OH was of the order of 100 ± 30 days for the high-latitude atmospheric conditions encountered. This lifetime is significantly longer than those estimated for the other carbon-containing compounds discussed, but it is close to the longest PAN lifetimes estimated for the summertime troposphere near 6 km at high latitudes [*Singh et al.*, this issue (*b*)]. Average mixing ratios of C_2Cl_4 were correlated with those of PAN and O_3 (cf. Figure 13). These similarities in altitudinal trends may suggest these compounds shared either common source(s) (e.g., the result of industrial/urban emissions) or common sinks (e.g., lower altitude sinks such as surface deposition and low-altitude thermally induced loss of PAN). These trends could also simply represent a tendency for long-lived compounds to accumulate in the Arctic middle troposphere.

Unlike the correlations with PAN and NO_y, average mixing ratios of C_2Cl_4 were only slightly correlated with those of NO_y and CO. In addition, average mixing ratios of CO were correlated with those of NO_y, but not with those of PAN (cf. Figures 14*a* and 14*b*). This correlation between CO and NO_y was in contrast to other lower-latitude remote tropospheric measurements that have generally found little correlation between CO and NO_y for NO_y mixing ratios <1 ppbv [e.g., *Parrish et al.*, 1991; *Hübler et al.*, 1992]. The slope of the regression between average CO and NO_y mixing ratios (slope ~0.04 ppbv/pptv) was also about twofold to fourfold larger than the slope obtained from the portion of their mid-latitude measurements that did exhibit correlation for NO_y mixing ratios >1 ppbv [*Parrish et al.*, 1991]. This difference in slopes and the observation of correlation between CO and NO_y for NO_y mixing ratios <1 ppbv could

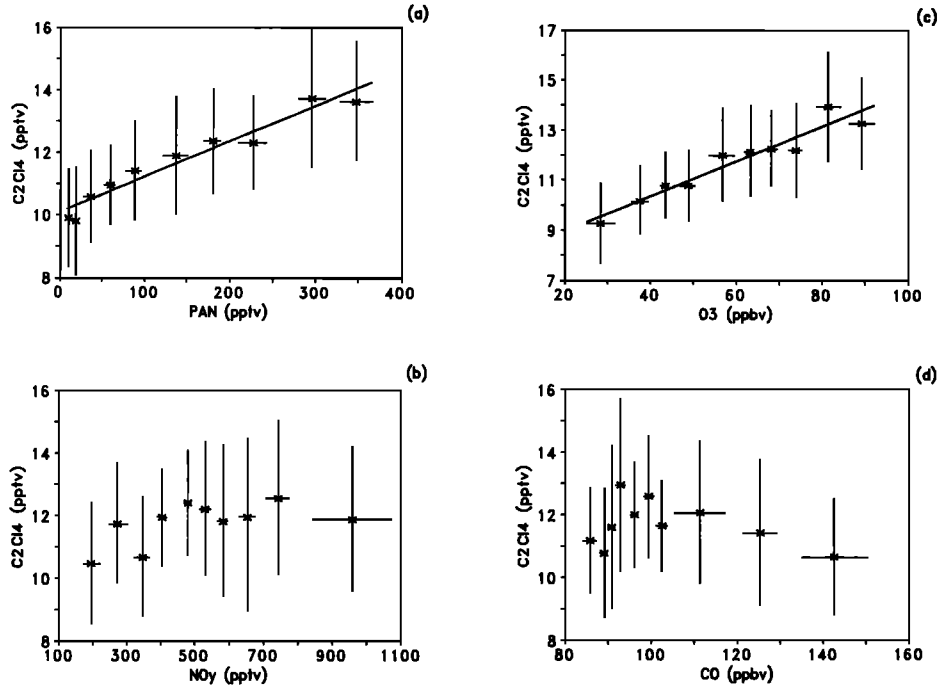

Fig. 13. Correlation plots for aggregated data, where the horizontal and vertical lines represent ±1 sigma about the mean of the aggregate: (*a*) C_2Cl_4 versus PAN with an aggregate size (AS) of 18 measurements (r^2 = 0.94 and slope of 0.0114 ± 0.001), (*b*) C_2Cl_4 versus NO_y with AS = 14 (r^2 = 0.34), (*c*) C_2Cl_4 versus O_3 with AS = 19 (r^2 = 0.92 and slope of 0.070 ± 0.007), and (*d*) C_2Cl_4 versus CO with AS = 17 (r^2 = 0.11).

suggest that the NO_y sources affecting these regions of Alaska were relatively close and favored smaller $\Delta NO_y/\Delta CO$ emission factors such as those expected from high-latitude biomass burning.

Even though they were not correlated with CO, average PAN mixing ratios were correlated with those of C_2H_2 (r^2 = 0.69) and with those of NO_y (r^2 = 0.80) (not shown here [see *Singh et al.*, this issue (*a*)]). These correlations along with those discussed earlier for C_2Cl_4 have been suggested to imply anthropogenic origins for these compounds [*Singh et al.*, this issue (*a*)]. However, the elapsed time for a 1/*e*-fold change in either PAN or NO_y mixing ratios ($\Delta t \sim 5$ days), implied from the regression of ln (C_2H_2/CO) versus PAN or NO_y, was significantly shorter than the estimated 15- to 30-day transport times from mid-latitude source regions (see section 4.2.4).

The elapsed times implied from the regressions of ln (C_2H_2/CO) versus PAN and NO_y were also significantly shorter than the NO_y lifetime estimated by *Jacob et al.* [this issue]. This estimate was based on assuming deposition of HNO_3 as the only sink of NO_y and setting the calculated rate of HNO_3 production equal to its deposition loss ($\Delta t \sim 18$ days for 1/*e*-fold change [*Jacob et al.*, this issue]). This estimated NO_y deposition flux balanced oxidation of NO_2 derived from the PAN reservoir within the column. This flux ($\sim 2.3 \times 10^9$ molecules cm^{-2} s^{-1}) was close to that measured for dry deposition near Bethel ($2 \pm 1 \times 10^9$ molecules cm^{-3} s^{-1}), even though approximately one-half of the measured deposition flux was attributed to compounds other than HNO_3, PAN, and NO_x [*Bakwin et al.*, this issue]. However, the estimated NO_3^- wet deposition flux for this region ($\sim 4 \times 10^9$ molecules cm^{-2} s^{-1}) was approximately twofold larger than the NO_y dry deposition flux [*Talbot et al.*, this issue]. NO_3^--containing aerosols contributed only a small fraction to the measured NO_y budget over Alaska (S. Sandholm et al., submitted manuscript, 1992). This suggests only a small fraction of the wet deposition flux was due to the local washout of NO_3^--containing aerosols. The lack of localized influences is also implied from the overall loss of NO_y obtained from combining the average wet and dry deposition fluxes to the average lower 6-km NO_y abundance, which yields a 1/*e*-folding time ($\Delta t \sim 6$ days) close to that implied from the regression of ln (C_2H_2/CO) versus NO_y. In addition, the similar regression obtained for ln (C_2H_2/CO) versus PAN suggests a large portion of the abundance of PAN may be attributable to short-range sources. A similar analysis using ln (C_3H_8/C_2H_6) as a surrogate for air mass aging (or transport time) did not yield significant correlations between ln (C_3H_8/C_2H_6) and PAN or NO_y ($r^2 < 0.3$). This lack of correlation may have been due to influx of C_3H_8 and C_2H_6 from noncombustion sources (see previous discussion in section 4.2.4). We readily admit that other interpretations of these trends are possible. Even so, these trends suggest short-range sources ($\Delta t \sim 6$ days) may have contributed substantially to the burden of N_xO_y compounds within the lower troposphere over Alaska and may have accounted for a large fraction of the NO_3 wet deposition flux measured over Bethel.

4.2.6. *Segregation of composites based on air mass type.* To further elucidate the factors contributing to the species distributions and correlative tendencies discussed throughout section 4, we segregated the composite data set using both chemical and meteorological criteria. The results of these segregation schemes are summarized in Table 2, where median values of each species or parameter are given for three altitude ranges above the mixed layer.

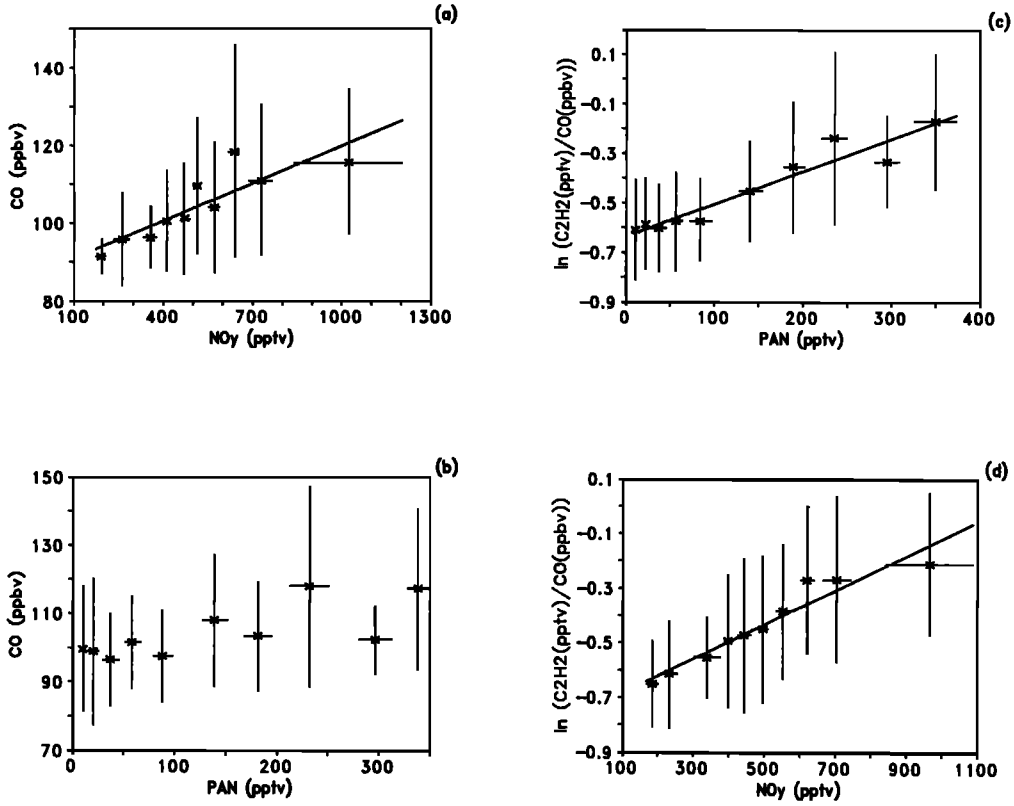

Fig. 14. Correlation plots of aggregated data, where the horizontal and vertical lines represent ±1 sigma about the mean of the aggregate: (*a*) CO versus NO_y with an aggregate size (AS) of 30 measurements ($r^2 = 0.75$ and slope of 0.032 ± 0.0065), =(b) CO versus PAN with AS = 17 ($r^2 = 0.56$ and slope of 0.050 ± 0.016), (*c*) ln (C_2H_2/CO) versus PAN with AS = 12 ($r^2 = 0.92$ and slope of 0.00132 ± 0.00014), (*d*) ln (C_2H_2/CO) versus NO_y with AS = 19 ($r^2 = 0.93$ and slope of $6.3 \times 10^{-4} \pm 6.3 \times 10^{-5}$).

The chemically based segregation schemes used either CO or O_3 mixing ratios as surrogates for defining "background" air. In the first case, background air was defined by mixing ratios of CO ≤ 110 ppbv (designated as CP-Bkg). This cutoff value for CO mixing ratios was selected based on the general trends described in section 4.2.1. The air masses characterized as plumes represent air with CO mixing ratios >115 ppbv. The second chemically derived case was adopted from the analyses of *Browell et al.* [this issue]. In this scheme (O_3-Bkg) background air was defined by mixing ratios of $O_3 < 35 + 9z$ (where z is altitude in kilometers) and mixing ratios of CO < 115 ppbv (used as a plume filter in place of relative aerosol scattering). Similarly, air of tropopausal origin (termed Strat.) was defined by mixing ratios of $O_3 > 35 + 9z$ and CO < 115 ppbv.

The meteorologically based segregation schemes used the 3- to 5-day back trajectory analyses of *Shipham et al.* [this issue] and the GTE data archive. This segregation scheme only used those portions of the composite data set where the air mass origin appeared to be well defined (e.g., no indication of split flow). This approach produced general regions of air mass origin defined as (1) air originating from west of 180°W and between 58° and 68°N, termed mid-Siberian (mid-Sib); (2) air originating from west of 180°W between 68° and 80°N, termed north of Siberia (N-Sib); (3) air originating from between 180° and 120°W and >73°N, termed Arctic pack ice (Pk-Ice); and (4) air originating between 140°–180°W and <55°N, termed Gulf of Alaska (Gulf AK).

As might be expected, the air masses originating from the Gulf of Alaska possessed a chemical signature with median mixing ratios of nearly all trace gases that were smaller than those in other air mass categories or in the overall composite (Comp). The significantly smaller (twofold to threefold) mixing ratios of PAN accounted for most of the reduction in median NO_y mixing ratios, as evidenced by the small median values of the ratio PAN/NO_y. The smaller median PAN mixing ratios found the Gulf of Alaska air masses are believed to represent the general lack of N_xO_y sources from this region, since median temperatures do not support enhanced thermal decomposition rates of PAN within these air masses. In general, the smaller median mixing ratios of C_2H_2, C_2H_6, and C_3H_8 also support the idea that these air masses were relatively disconnected from these compounds' sources. During summer, approximately 45% of the air masses influencing western Alaska originate from sectors covering the North Pacific Ocean. Taking this fraction, in conjunction with the somewhat smaller median NO_y mixing ratios, suggests that about 35% of the middle tropospheric NO_y burden may have originated from these regions. This fraction may represent the contribution of relatively well-aged lower-latitude background air.

In contrast to the Gulf of Alaska air masses, those categorized as plumes possessed a chemical signature with median mixing ratios of nearly all trace gases that were larger than those in the overall composite or in most of the other air mass categories. Median PAN mixing ratios were

particularly enhanced within the lowest altitude range. This enhancement, despite the warmer air temperatures, suggest that N_xO_y emissions from short-range sources were responsible for these observations. In addition, the significantly enhanced median NO_y mixing ratios within this air mass category indicate a large fraction of the NO_y budget consisted of compounds other than NO_x and PAN.

The air masses categorized as originating from mid-Siberia possessed a chemical signature nearly identical to that found for the plumes. In particular, median values of potential temperature, CO, and H_2O are remarkably similar in comparison to median values for the other air mass categories. The smaller median value of PAN within the lowest altitude range may represent the thermal loss of this reservoir compound during transport over the relatively N_xO_y-sourceless Bering Sea. This result also supports the earlier suggestion that some of the enhancement in PAN mixing ratios, in the plume categorized air masses, may have originated from more localized N_xO_y emissions. The larger median values of the ratios C_2H_2/CO and C_3H_8/C_2H_6 also imply that these two air mass categories are similar. These ratios also suggest a relatively young age for these two air mass categories.

In the companion paper of *Jacob et al.* [this issue], high-latitude biomass burning emissions were argued to have had only a small affect (~20%) on the abundance of CO and NO_y for the high-latitude regions as a whole (taken as >60°N). This analysis was based on an estimated CO inventory from biomass burning of about 4 Tg for fires north of 60°N, which yielded an average CO flux of about 1×10^{11} molecules cm^{-2} s^{-1}. Using the average $\Delta NO_y/\Delta CO$ emission factor obtained from the Kuskokwim Delta region [*Wofsy et al.*, this issue], it was argued that the equivalent NO_y emission flux ($\sim 5 \times 10^8$ molecules cm^{-2} s^{-1}) could only have balanced about 20% of the estimated dry deposition NO_y sink. This estimate would then correspond to balancing only about 7% of the estimated total dry and wet deposition fluxes discussed earlier.

Regionally, however, high-latitude biomass burning could have a substantially larger impact. In particular, approximately 50% of high-latitude biomass burning is believed to occur in Siberia [*Stocks*, 1991]. Most of central Siberia was predominantly under the influence of high pressure during July and August 1988. This could suggest that relatively dry conditions prevailed, and that 1988 may have represented at least an average fire season throughout Siberia. Spreading this source's influence over the more limited area covering a westward flow path to Alaska ($\sim 7 \times 10^6$ km^2 versus 3.5×10^7 km^2 for the northern hemisphere >60°N) would result in an equivalent NO_y source flux of about 2.5×10^9 molecules cm^{-2} s^{-1}. This flux could balance nearly all of the estimated NO_y dry deposition flux and about 35% of the estimated total dry and wet deposition fluxes. If a twofold to threefold larger $\Delta NO_y/\Delta CO$ emission factor applies to taiga fires, as might be suggested by the plumes encountered on mission 6, then nearly 80% of the total dry and wet deposition flux could be balanced from the Siberian biomass burning source. These estimates suggest biomass burning may have been an extremely important regional-scale source for air originating from central Siberia.

During summer, approximately 20% of the air masses influencing western Alaska originate from sectors that could be affected by mid-Siberian emissions. Considering this contribution along with the nearly 1.5-fold larger median NO_y mixing ratios found in air masses from this sector suggests that about 30% of the NO_y burden over western Alaska could be due to biomass burning in mid-Siberia. This burden could be in addition to any general enhancement background in high-latitude NO_y mixing ratios due to biomass burning. This estimate of the NO_y burden due to biomass burning is in agreement with the multivariant analyses of *Wofsy et al.* [this issue]. This NO_y burden is, however, a larger contribution than might be implied from the analyses of *Browell et al.* [this issue], in which the fraction of air masses containing discrete haze layers was of the order of 10%. However, the fraction of this composite data set containing chemically enhanced air with CO mixing ratios >115 ppbv was approximately 22%, suggesting that cloud processing of aerosol (i.e., removal) may have contributed to an underestimate of "plumes" based on lidar aerosol-scattering measurements. Indeed, several chemically enhanced layers were encountered that contained very small enhancements in aerosol number densities.

Air masses originating from north of Siberia and from the Arctic pack ice should have been relatively free from the short-range effects of biomass burning. The larger median mixing ratios of C_2Cl_4 found in higher altitudes suggest these air mass categories may reveal the chemical signature associated with long-range transport from European and North American industrial regions. This, coupled with the average frequency of occurrence of air masses originating from these sectors (~30%), could suggest that about 35% of the NO_y burden over western Alaska could have also been due to the long-range transport of pollutants from lower latitude industrial/urban regions. However, downward transport of tropopausal NO_y may have contributed to a portion of the NO_y in these and other air mass categories, which originated from regions with larger frequencies of occurrence of enhanced potential vorticity.

The air categorized as originating from downward transport of tropopausal air (Strat in Table 2) did not exhibit a chemical signature markedly different from the other air mass categories, except for the plume and mid-Siberian types. This could represent the loss of a distinct stratospheric signature as the air was advected during transport and mixed with upper/middle tropospheric air. Alternatively, the lack of a distinct signature could imply that high-latitude tropopausal air possesses a chemical signature closer to that of tropospheric air, with the exception of enhanced O_3 mixing ratios derived from the stratosphere.

We can only speculate on the chemical characteristics of the tropospheric air residing above 6 km over these regions. However, if the springtime high-latitude NO_y profiles measured by *Dickerson* [1985] are paradigmatic, then continued increases in proportion to altitude in the mixing ratios of many compounds, especially NO_y, should not necessarily be expected for the upper troposphere. Based on Dickenson's measurements, a substantial reduction in NO_y mixing ratios may occur between 6 km and the air above. This coupled with the trends described in the case studies suggest the influx of tropopausal air could be an important source of NO_y into the region. Even so, it would seem unlikely that the middle stratosphere is the ultimate source of this NO_y, based on the case studies presented, unless an efficient means of converting stratospheric HNO_3 into other N_xO_y compounds exists. This adumbrates other N_xO_y sources

TABLE 2. Characterization of Air Masses Constituting the Vertical Composite

Altitude, km	Comp.	CO Bkg	Plume	O_3 Bkg	Strat	Mid-Sib	N-Sib	Pk-Ice	Gulf AK
				NO, pptv					
2.25	8	6.8	9.8	6.3	11.5	9.5	5.5	5.7	7.3
3.75	9.2	9.1	10	8.7	11	13	12	7	6.8
5.3	8.3	8.2	9.7	7.3	8.6	17	8.9	7.5	4.8
				NO_x, pptv					
2.25	22	22	28	19	37	19	22	21	18
3.75	27	23	34	21	28	28	24	22	20
5.3	25	25	26	24	32.5	36	24	23	27
				PAN, pptv					
2.25	67	65	190	50	99	88	60	33	44
3.75	180	170	240	140	220	150	200	210	75
5.3	300	280	340	220	310	450	280	280	94
				NO_y, pptv					
2.25	420	380	700	380	400	630	300	525	380
3.75	570	500	705	500	525	1000	500	630	470
5.3	610	610	710	600	620	950	620	750	390
				NO_x/NO_y, pptv/pptv*					
2.25	0.06	0.07	0.035	0.05	0.09	0.033	0.08	0.043	0.048
3.75	0.05	0.05	0.036	0.044	0.053	0.027	0.05	0.037	0.047
5.3	0.04	0.04	0.036	0.042	0.049	0.039	0.04	0.043	0.046
				PAN/NO_y, pptv/pptv*					
2.25	0.21	0.19	0.24	0.16	0.31	0.13	0.23	0.15	0.13
3.75	0.36	0.36	0.31	0.24	0.40	0.22	0.48	0.36	0.22
5.3	0.47	0.44	0.57	0.48	0.53	0.43	0.52	0.43	0.25
				O_3, ppbv					
2.25	53	53	60	47	64	51	47	60	45
3.75	70	69	73	61	79	74	73	79	47
5.3	77	79	73	75	89	92	78	90	44
				CO, ppbv					
2.25	98	95	137	91	98	135	89	97	100
3.75	100	97	138	97	99	139	94	99	94
5.3	102	98	125	100	100	123	98	95	91
				C_2H_2, pptv					
2.25	53	49	120	48	53	110	52	48	56
3.75	65	61	170	61	64	130	66	60	48
5.3	79	65	120	71	62	110	85	65	52
				C_2H_6, pptv					
2.25	833	811	983	810	833	956	852	833	715
3.75	853	847	1104	836	861	1003	891	875	742
5.3	932	885	1042	909	885	991	940	884	710
				C_3H_8, pptv					
2.25	84	78	116	80	77	119	86	66	94
3.75	80	75	136	75	77	144	69	77	73
5.3	103	92	161	92	96	143	94	80	83
				C_2Cl_4, pptv					
2.25	12	12	11	12	12	10	12	12	10
3.75	12	13	11	12	13	10	14	13	10
5.3	13	13	13	14	13	12	15	15	12
				NO_yO_3, pptv/pptv*					
2.25	0.0072	0.0067	0.0125	0.0076	0.0062	0.0121	0.0065	0.0092	0.0095
3.75	0.0076	0.0070	0.0097	0.0078	0.0067	0.0139	0.0063	0.0093	0.0094
5.3	0.0080	0.0079	0.0090	0.0082	0.0071	0.0123	0.0079	0.0091	0.0088
				C_2H_2/CO, pptv/ppbv*					
2.25	0.55	0.50	0.83	0.50	0.54	0.82	0.56	0.50	0.56
3.75	0.68	0.64	1.14	0.66	0.66	0.97	0.57	0.61	0.51
5.3	0.73	0.65	0.93	0.71	0.64	0.92	0.70	0.71	0.54
				C_3H_8/C_2H_6, pptv/pptv*					
2.25	0.11	0.10	0.12	0.10	0.096	0.13	0.10	0.081	0.12
3.75	0.10	0.092	0.13	0.16	0.090	0.14	0.077	0.093	0.097
5.3	0.12	0.11	0.17	0.11	0.12	0.15	0.10	0.094	0.11

TABLE 2. (continued)

Altitude, km	Comp.	CO Bkg	Plume	O_3 Bkg	Strat	Mid-Sib	N-Sib	Pk-Ice	Gulf AK
				Temperature, °C					
2.25	1.5	0.5	4	−0.03	0.88	4.1	−1.3	−2.6	−1.2
3.75	−6.5	−7.6	−3.5	−8.3	−6.4	−1	−10	−9.7	−5.2
5.3	−16	−17	−13	−16	−17	−14	−23	−21	−16
				H_2O, pptv					
2.25	5.0	4.8	6.9	6.0	2.6	6.9	5.7	2.3	5.7
3.75	2.4	2.0	4.2	3.0	1.4	4.9	1.5	1.4	3.1
5.3	0.90	0.82	2.3	0.90	0.67	1.5	0.63	0.5	1.6
				Potential Temperature, K					
2.25	296	296	301	295	297	301	294	294	295
3.75	304	303	309	303	303	307	302	300	299
5.3	311	310	314	309	311	315	310	306	308

*Median values are of ratios, not ratios of medians.

may have contributed significantly to the tropopausal abundance of NO_y.

The contribution of high-altitude aircraft emissions, which have large $\Delta NO_y/\Delta CO$ emission factors, could be one such source [*Ehhalt et al.*, 1992]. This source would correspond to the characteristics needed to provide the portion (30–45%) of NO_y mixing ratios analyzed as stratospheric that were highly correlated with those of O_3 but not with those of CO [*Wofsy et al.*, this issue].

However, if an efficient mechanism exists within the tropopause for converting HNO_3 into other long-lived N_xO_y reservoir compounds, then a corresponding large fraction of the NO_y burden with the troposphere's lower 6 km may have been derived from the stratosphere. Approximately 50% of the air masses encountered were indicated as having stratospheric character [*Browell et al.*, this issue]. In such cases, conservation of the stratospheric HNO_3 pool of N_xO_y could provide the large stratospheric NO_y contribution (30–45%). The corollary argument could, however, imply that an equally large fraction may be due to sources such as high-altitude aircraft emissions.

Significant uncertainty (perhaps twofold) exists in all of the estimates discussed above. Even so, these analyses are believed to depict at least a semiquantitative estimate of the factors controlling the summertime abundance of N_xO_y compounds over western Alaska. In particular, the largest degree of uncertainty is involved in assessing the relative contribution from anthropogenic sources. If the median mixing ratios of CO measured within the Gulf of Alaska air masses represent a relative baseline for comparing the impact from lower latitude sources, then for CO mixing ratios of 90–100 ppbv, approximately 200–400 pptv of NO_y could be attributable to anthropogenic sources based on the regression discussed earlier. This would predict that somewhere between one- and two-thirds of the abundance of NO_y could have originated from such sources. In conjunction, about one-third to one-half of the NO_y is indicated as having originated from biomass burning and another one-third to one-half as having originated from the downward transport of tropopausal air.

5. SUMMARY

We have attempted to assess the factors that control the abundance of N_xO_y compounds in the lower 6-km tropospheric column over Alaska. Our analyses identified several potential factors that may significantly influence tropospheric chemistry over this region. The most prominent of these are posed below in the form of questions.

1. What are the chemical characteristics of the summertime high-latitude tropospheric column above 6 km, and of the tropopausal region?
2. Is there an efficient mechanism for converting stratospherically derived HNO_3 into other NO_x-containing reservoir compounds?
3. To what extent does the 3- to 6-km altitude region at high latitudes represent a "stable" regime for accumulating surface-emitted pollutants and O_3 from aloft?
4. How variable are emission factors of trace gases from high-latitude biomass burning, especially throughout the vast regions of Siberia?
5. How important are the anthropogenic N_xO_y source inventories for Siberia (or Russia)?
6. What compounds constitute the large fraction of NO_y not accounted for by NO_x, PAN, and HNO_3? How "reactive" a form of odd nitrogen are they?
7. How extensive and variable are quasi-localized regions of enhanced potential vorticity and how well do these regions reflect patterns of stratospheric/tropospheric exchange? What is the climatology of summertime high-latitude stratospheric/tropospheric exchange (see also similar question by *Staehelin and Schmid* [1991])? How would quasi-localized areas of enhanced exchange affect the interpretation of current ozonesonde data bases?
8. How important are the observed long-term trends in high-latitude biomass burning to the chemical climatology over high latitudes? Are the temporally coincident long-term tendencies in high-latitude biomass burning and enhanced middle-tropospheric ozone potentially caused by climate changes [cf. *Van Wagner*, 1988; *Logan*, 1985]? Are these trends in burned areas associated with climatological patterns that may suggest large-scale atmosphere/biosphere couplings?

These questions are important, and their answers should be addressed in future modeling and field program activities.

Acknowledgments. The authors are extremely grateful to the pilots and crew of the Wallops flight facility Electra for their dedication during this safe and successful field program and for their

patience in enduring the many slow spiral descents that are featured in this article. We are especially grateful to Roger Navarro, Jim Hoell, Richard Bendura, Joseph Drewry, and Helen Thompson for coordination of the operational and logistical support that was so crucial to the success of this program. Our highest commendation goes to Bob Harriss for his ability as mission scientist to juggle the desires of the science team, the demands of the program goals, and the diversity of nature. We are also grateful to J. Ward, J. Bradbury, S. Simms, S. Shurling, and D. Yang for their contributions toward data analysis and preparation of this manuscript. This research program was sponsored by the National Aeronautics and Space Administration, Tropospheric Chemistry Program Office under the Program Directorship of Robert J. McNeal.

REFERENCES

Atherton, C. S., and J. E. Penner, The effect of biogenic hydrocarbons on the transformation of nitrogen oxides in the troposphere, *J. Geophys. Res.*, *95*, 14,027–14,038, 1990.

Atlas, E., Evidence for ≥C3 alkyl nitrates in rural and remote atmosphere, *Nature*, *331*, 426–430, 1988.

Bakwin, P. S., S. C. Wofsy, and S. Fan, Measurements of NO_x and NO_y concentrations and fluxes over Arctic tundra, *J. Geophys. Res.*, this issue.

Blake, D. R., et al., Summertime measurements of selected nonmethane hydrocarbons in the Arctic and sub-Arctic during the 1988 Arctic Boundary Layer Expedition (ABLE 3A), *J. Geophys. Res.*, this issue.

Bollinger, M. J., R. F. Sievers, D. W. Fahey, and F. C. Fehsenfeld, Conversion of nitrogen dioxide, nitric acid, and *n*-propyl nitrate to nitric oxide by gold catalyzed reduction with carbon monoxide, *Anal. Chem.*, *55*, 1980–1986, 1983.

Bradshaw, J. D., M. O. Rodgers, S. T. Sandholm, S. Kesheng, and D. D. Davis, A two-photon laser-induced fluorescence field instrument for ground based and airborne measurements of atmospheric NO, *J. Geophys. Res.*, *90*, 12,861–12,873, 1985.

Brock, C. A., L. F. Radke, J. H. Lyons, and P. V. Hobbs, Arctic hazes in summer over Greenland and the North American Arctic, I, Incidence and origins, *J. Atmos. Chem.*, *9*, 129–148, 1989.

Browell, E. V., C. F. Butler, S. A. Kooi, M. A. Fenn, R. C. Harriss, and G. L. Gregory, Large-scale variability of ozone and aerosols in the summertime Arctic and sub-Arctic troposphere, *J. Geophys. Res.*, this issue.

Carlson, T. N., Speculations on the movement of polluted air to the Arctic, *Atmos. Environ.*, *15*, 1473–1477, 1981.

Carroll, M. A., et al., Aircraft measurements of NO_x over the eastern Pacific and continental United States and implications for ozone production, *J. Geophys. Res.*, *95*, 10,205–10,233, 1990.

Chameides, W. L., et al., Observed and model-calculated NO_2/NO ratios in tropospheric air sampled during the NASA GTE/CITE 2 field study, *J. Geophys. Res.*, *95*, 10,235–10,247, 1990.

Chapin, F. S., III, and G. R. Shaver, *Physiological Ecology of North American Plant Communities*, Chapman Hall, London, 1985.

Crutzen, P. J., The role of NO and NO_2 in the chemistry of the troposphere and stratosphere, *Annu. Rev. Earth Planet. Sci.*, *7*, 443–472, 1979.

Danielson, E. F., Stratospheric-tropospheric exchange based on radioactivity, ozone, and potential vorticity, *J. Atmos. Sci.*, *25*, 502–518, 1968.

Demerjian, K. L., K. L. Schere, and J. T. Peterson, Theoretical estimates of actinic (spherically integrated) flux and photolytic rate constants of atmospheric species in the lower troposphere, *Adv. Environ. Sci. Technol.*, *10*, 396–459, 1980.

DeMore, W. B., S. P. Sander, M. J. Molina, D. M. Golden, R. F. Hampson, M. J. Kurylo, C. J. Howard, and A. R. Ravishankara, Chemical kinetics and photochemical data for use in stratospheric modeling, Evaluation 9, *JPL Publ.*, *90-91*, 1990.

Dickerson, R. R., Reactive nitrogen compounds in the Arctic, *J. Geophys. Res.*, *90*, 10,739–10,743, 1985.

Doskey, P. V., and J. S. Gaffney, Nonmethane hydrocarbons in the Arctic atmosphere at Barrow, Alaska, *Atmos. Environ.*, *19*, 381–384, 1992.

Douglass, A. R., C. H. Jackman, and R. S. Stolarski, Comparison of model results transporting the odd nitrogen family with results transporting separate odd nitrogen species, *J. Geophys. Res.*, *94*, 9862–9872, 1989.

Ebel, A., H. Hass, H. J. Jakobs, M. Laube, M. Memmesheimer, A. Oberreuter, H. Geiss, and Y. H. Kuo, Simulation of ozone intrusion caused by a tropopause fold and cut-off low, *Atmos. Environ.*, *25*, 2131–2144, 1991.

Ehhalt, D. H., F. Rohrer, and A. Wahner, Sources and distribution of NO_x in the upper troposphere at northern mid-latitudes, *J. Geophys. Res.*, *97*, 3725–3738, 1992.

Fahey, D. W., C. S. Eubanks, G. Hübler, and F. C. Fehsenfeld, Evaluation of a catalytic reduction technique for the measurement of total reactive odd-nitrogen NO_y in the atmosphere, *J. Atmos. Chem.*, *3*, 435–468, 1985.

Fehsenfeld, F. C., et al., Intercomparison of NO_2 measurement techniques, *J. Geophys. Res.*, *95*, 3579–3597, 1990.

Gidel, L. T., and M. A. Shapiro, General circulation model estimates of the net vertical flux of ozone in the lower stratosphere and the implications for the tropospheric ozone budget, *J. Geophys. Res.*, *85*, 4049–4058, 1980.

Gregory, G. L., J. M. Hoell, Jr., A. L. Torres, M. A. Carroll, B. A. Ridley, M. O. Rodgers, J. D. Bradshaw, S. T. Sandhom, and D. D. Davis, An intercomparison of airborne nitric oxide measurements: A second opportunity, *J. Geophys. Res.*, *95*, 10,129–10,138, 1990*a*.

Gregory, G. L., et al., An intercomparison of airborne nitrogen dioxide instruments, *J. Geophys. Res.*, *95*, 10,103–10,127, 1990*b*.

Gregory, G. L., B. E. Anderson, L. S. Warren, E. V. Browell, D. R. Bagwell, and C. H. Hudgins, Tropospheric ozone and aerosol observations: The Alaskan Arctic, *J. Geophys. Res.*, this issue.

Harriss, R. C., et al., The Arctic Boundary Layer Expedition (ABLE 3A): July–August 1988, *J. Geophys. Res.*, this issue (*a*).

Harriss, R. C., G. W. Sachse, G. F. Hill, L. Wade, K. B. Bartlett, J. E. Collins, P. Steele, and P. Novelli, Carbon monoxide and methane in the North American Arctic and sub-Arctic troposphere: July–August 1988, *J. Geophys. Res.*, this issue (*b*).

Hübler, G., et al., Total reactive oxidized nitrogen (NO_y) in the remote Pacific troposphere and its correlation with O_3 and CO: Mauna Loa Observatory Photochemistry Experiment 1988, *J. Geophys, Res.*, *97*, 10,427–10,447, 1992.

Hoell, J. M., et al., An intercomparison of carbon monoxide, nitric oxide, and hydroxyl measurement techniques: Overview results, *J. Geophys. Res.*, *89*, 11,819–11,825, 1984.

Hoell, J. M., G. L. Gregory, D. S. McDougal, A. L. Torres, D. D. Davis, J. D. Bradshaw, M. O. Rodgers, B. A. Ridley, and M. A. Carroll, Airborne intercomparison of nitric oxide measurement techniques, *J. Geophys. Res.*, *92*, 1995–2008, 1987.

Jacob, D. J., et al., Summertime photochemistry of the troposphere at high northern latitudes, *J. Geophys. Res.*, this issue.

Kondo, Y., P. Aimedieu, W. A. Matthews, W. R. Sheldon, and J. R. Benbrook, A mid-latitude balloon-borne observation of total odd nitrogen, *Geophys. Res. Lett.*, *17*, 73–76, 1990.

Levy, H., II, Photochemistry of the lower troposphere, *Planet. Space Sci.*, *20*, 919–935, 1972.

Levy, H., II, and W. J. Moxim, Influence of long-range transport on the chemical variability of the background atmosphere, *Nature*, 338, 326–328, 1989.

Lin, X., M. Trainer, and S. C. Liu, On the nonlinearity of the tropospheric ozone production, *J. Geophys. Res.*, *93*, 15,879–15,888, 1988.

Liu, S. C., M. Trainer, F. C. Fehsenfeld, D. D. Parrish, E. J. Williams, D. W. Fahey, G. Hübler, and P. C. Murphy, Ozone production in the rural troposphere and the implications for regional and global ozone distributions, *J. Geophys. Res.*, *92*, 4191–4207, 1987.

Logan, J. A., Nitrogen oxides in the troposphere: Global and regional budgets, *J. Geophys. Res.*, *88*, 10,785–10,807, 1983.

Logan, J. A., Tropospheric ozone: Seasonal behavior, trends, and anthropogenic influence, *J. Geophys. Res.*, *90*, 10,463–10,482, 1985.

Logan, J. A., M. J. Prather, S. C. Wofsy, and M. B. McElroy, Tropospheric chemistry: A global perspective, *J. Geophys. Res.*, *86*, 7210–7254, 1981.

Madronich, S., and J. C. Calvert, Permutation reactions of organic peroxyl radicals in the troposphere, *J. Geophys. Res.*, *95*, 5697–5715, 1990.

McFarland, M., D. Kley, J. W. Drummond, A. L. Schmeltekopf, and R. H. Winkler, Nitric oxide measurements in the equatorial Pacific region, *Geophys. Res. Lett.*, *6*, 605–608, 1979.

Miller, J. M., A five-year climatology of five-day back trajectories from Barrow, Alaska, *Atmos. Environ.*, *15*, 1401–1405, 1981.

Moxim, W. J., Simulated transport of NO_y to Hawaii during August: A synoptic study, *J. Geophys. Res.*, *95*, 5697–5715, 1990.

Murphy, D. M., and D. W. Fahey, Mathematical treatment of the wall loss of a trace species in denuder and catalytic converter tubes, *Anal. Chem.*, *59*, 2753–2759, 1987.

Murphy, D. M., D. W. Fahey, M. H. Proffitt, S. C. Liu, K. R. Chan, C. S. Eubank, S. R. Kawa, and K. K. Kelley, Reactive nitrogen and its correlation with ozone in the lower stratosphere and upper troposphere, *J. Geophys. Res.*, in press, 1992.

National Academy of Sciences, *Alternative Fuels for Maritime Use*, National Academy of Science Press, Washington, D. C., 1980.

Parrish, D. D., P. C. Murphy, D. L. Albriton, and F. C. Fehsenfeld, The measurement of photodissociation rate of NO_2 in the atmosphere, *Atmos. Environ.*, *15*, 1439–1445, 1981.

Parrish, D. D., M. Trainer, M. Buhr, B. A. Watkins, and F. C. Fehsenfeld, Carbon monoxide concentrations and their relation to concentrations of total reactive oxidized nitrogen at two rural U.S. sites, *J. Geophys. Res.*, *96*, 9309–9320, 1991.

Patterson, D. E., and R. B. Husar, A direct simulation of hemispherical transport of pollutants, *Atmos. Environ.*, *15*, 1479–1482, 1981.

Porch, W. M., C. J. Kao, and R. G. Kelley, Jr., Ship trails and ship-induced cloud dynamics, *Atmos. Environ.*, *24*, 1051–1059, 1990.

Raatz, W. E., R. C. Schnell, B. A. Bodhaine, S. J. Oltmans, and R. H. Gammon, Air mass characteristics in the vicinity of Barrow, Alaska, 9–19 March 1983, *Atmos. Environ.*, *19*, 2127–2134, 1985.

Rahn, K. A., Relative importance of North America and Eurasia as sources of Arctic aerosol, *Atmos. Environ.*, *15*, 1447–1455, 1981.

Reiter, E. R., Stratospheric-tropospheric exchange processes, *Rev. Geophys.*, *13*, 459–474, 1975.

Ridley, B. A., M. A. Carroll, G. L. Gregory, and G. W. Sachse, NO and NO_2 in the troposphere: Technique and measurements in regions of a folded tropopause, *J. Geophys. Res.*, *93*, 15,813–15,830, 1988.

Ridley, B. A., M. A. Carroll, D. D. Dunlap, M. Trainer, G. W. Sachse, G. L. Gregory, and E. P. Condon, Measurements of NO_x over the eastern Pacific Ocean and southwestern United States during the spring 1984 NASA GTE aircraft program, *J. Geophys. Res.*, *94*, 5043–5067, 1989.

Russell, J. M., III, C. B. Farmer, C. P. Rinsland, R. Zander, L. Froidevaux, G. C. Toon, B. Gao, J. Shaw, and M. Gunson, Measurements of odd nitrogen compounds in the stratosphere by the ATMOS experiment on Spacelab 3, *J. Geophys. Res.*, *93*, 1718–1736, 1988.

Sandholm, S. T., J. D. Bradshaw, K. S. Dorris, M. O. Rodgers, and D. D. Davis, An airborne compatible photofragmentation two-photon laser-induced fluorescence instrument for measuring background tropospheric NO, NO_x, and NO_2, *J. Geophys. Res.*, *95*, 10,155–10,161, 1990.

Shapiro, M. A., T. Hampel, and A. J. Krueger, The arctic tropopause fold, *Mon. Weather Rev.*, *115*, 444–454, 1987.

Shaw, G. E., Eddy diffusion transport of arctic pollution from the mid-latitudes: A preliminary model, *Atmos. Environ.*, *15*, 1483–1490, 1981.

Shaw, G. E., Chemical air mass systems in Alaska, *Atmos. Environ.*, *22*, 2239–2248, 1988.

Shipham, M. C., A. S. Bachmeier, D. R. Cahoon, Jr., and E. V. Browell, Meteorological overview of the Arctic Boundary Layer Expedition (ABLE 3A) flight series, *J. Geophys. Res.*, this issue.

Singh, H. B., Reactive nitrogen in the troposphere, *Environ. Sci. Technol.*, *21*, 320–327, 1987.

Singh, H. B., and P. L. Hanst, Peroxyacetyl nitrate (PAN) in the unpolluted troposphere: An important reservoir for nitrogen oxides, *Geophys. Res. Lett.*, *8*, 941–944, 1981.

Singh, H. B., and L. J. Salas, Peroxyacetyl nitrate in the free troposphere, *Nature*, *302*, 326–328, 1983.

Singh, H. B., and P. B. Zimmerman, Atmospheric distribution and sources of nonmethane hydrocarbons, in *Gaseous Pollutants: Characterization and Cycling*, John Wiley, New York, 1992.

Singh, H. B., D. O'Hara, D. Herlth, J. D. Bradshaw, S. T. Sandholm, G. L. Gregory, G. W. Sachse, D. R. Blake, P. J. Crutzen, and M. A. Kanakidou, Atmospheric measurements of peroxyacetyl nitrate and other organic nitrates at high latitudes: Possible sources and sinks, *J. Geophys. Res.*, this issue (*a*).

Singh, H. B., D. Herlth, D. O'Hara, K. Zahnle, J. D. Bradshaw, S. T. Sandholm, R. Talbot, P. J. Crutzen, and M. Kanakidou, Relationships of peroxyacetyl nitrate to active and total odd nitrogen at northern high latitudes: Influence of reservoir species on NO_x and O_3, *J. Geophys. Res.*, this issue, (*b*).

Staehelin, J., and W. Schmid, Trend analysis of tropospheric ozone concentrations utilizing the 20-year data set of ozone balloon soundings over Payerne (Switzerland), *Atmos. Environ.*, *25*, 1739–1749, 1991.

Stocks, B. J., The extent and impact of forest fire in northern circumpolar countries, in *Global Biomass Burning*, MIT Press, Cambridge, Mass., 1991.

Talbot, R. W., A. S. Vijgen, and R. C. Harriss, Soluble species in the Arctic summer troposphere: Acidic gases, aerosols and precipitation, *J. Geophys. Res.*, this issue.

U.S. Department of Transportation, *United States Oceanborne Foreign Trade Routes*, Washington, D. C., 1988.

Van Wagner, C. E., The historical pattern of annual burned area in Canada, *For. Chron.*, 1988.

Vaughan, G., and J. D. Price, Ozone transport into the troposphere in a cut-off low event, in *Ozone in the Atmosphere*, pp. 415–418, 1989.

Warneck, P., *Chemistry of the Natural Atmosphere*, Academic, San Diego, Calif., 1988.

Wofsy, S. C., et al., Atmospheric chemistry in the Arctic and sub-Arctic: Influence of natural fires, industrial emissions, and stratospheric inputs, *J. Geophys. Res.*, this issue.

A. S. Bachmeier, Planning Research Corporation, Hampton, VA 23665.

J. D. W. Barrick, E. V. Browell, G. L. Gregory, G. W. Sachse, and M. A. Shipham, NASA Langley Research Center, Hampton, VA 23665-5225.

D. R. Blake, Department of Chemistry, University of California at Irvine, Irvine, CA 92717.

J. D. Bradshaw, G. Chen, and S. T. Sandholm, School of Earth and Atmospheric Sciences, Georgia Institute of Technology, Atlanta, GA 30332.

D. Owen, S. T. Systems Corporation, Hampton, VA 23666.

H. B. Singh, NASA Ames Research Center, Moffett Field, CA 94035.

R. W. Talbot, Institute for the Study of Earth, Oceans, and Space, University of New Hampshire, Durham, NH 03824.

(Received June 20, 1991;
revised June 20, 1992;
accepted June 20, 1992.)